THOUNTHONG: MODEL BASED-ENERGY CONTROL OF A SOLAR POWER PLANT WITH A SUPERCAPACITOR

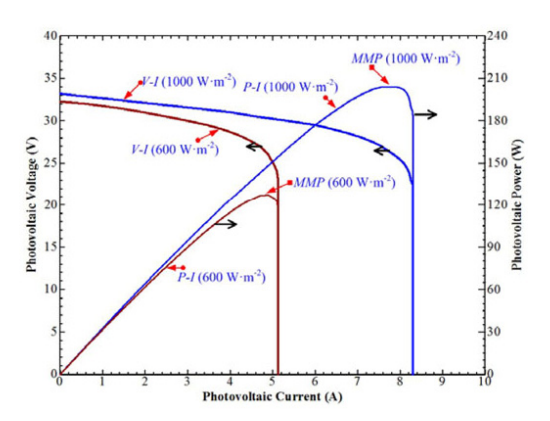


Fig. 1. Power versus current characteristics and voltage versus current characteristics based on a 200-W PV module by the Ekarat Solar at fixed ambient temperature and variable insolation (1000 and 600 W·m $^{-2}$).

dc voltage tracking control of a three-phase voltage source converter [21]; the control of open-channel flow in an irrigation canal [22]; and the current control for three-phase three-wire boost converters [23].

We now study an uncomplicated design of a control system of the PV/SC power plant based upon the physical structure of the model. The main contribution of this paper is to present the differential flatness-based control approach of a solar power generation system with an SC storage device. In particular, we do not restrict ourselves to linear control techniques at an equilibrium point. This is the novel work in this domain. The remaining of the paper is structured as follows: the next section describes the hybrid energy system and the power plant model that is studied in this work. In Section III, the proposed energy management algorithm is presented. In Section IV, a proof of the flat system consisting of the solar energy power plant, the control laws, and the system stability is presented. In Section V, the test bench results for the proposed system are presented. Finally, this paper ends with concluding remarks for further study in Section VI.

II. Power Source Characteristics

A. Photovoltaic

The PV effect is a basic physical process through which solar energy is converted directly into electrical energy. The physics of a PV cell, or solar cell, is similar to the classical p–n junction diode. The $V{-}I$ and $P{-}I$ characteristic curves of the PV model used in this study (200-W PV Module by the Ekarat Solar Company) under different irradiances (at 25 °C) are given in Fig. 1. As shown in Fig. 1, the higher the irradiance, the larger the short-circuit current $I_{\rm SC}$ and the open-circuit voltage $V_{\rm OC}$. As a result, the output PV power will also be larger.

Remark 1: PV power systems require some specific estimation algorithms to deliver the maximum power point (MPP) [24], [25]. Because of the typical low-efficiency characteristics of PV panels, it is very important to deliver the maximum instantaneous power from these energy sources to the load with minimum power conversion for space or terrestrial applications. Temperature also plays an important role in the PV array performance. The lower the temperature, the higher the maximum power and the larger the open-circuit voltage. It is obligatory to use dc/dc or dc/ac converters with effective MPP tracking (MPPT) techniques [26].

B. Supercapacitor

The SC (or double-layer capacitor or ultracapacitor) is an emerging technology in the field of energy-storage systems. Recent breakthroughs in construction methods aimed at maximizing rated capacitance have provided tremendous increases in the energy-storage capabilities of the double-layer capacitor [27]. With a time constant (the product of equivalent series resistance (ESR) and capacitance) of 0.001–2 s for an SC, the ESR inside an SC is very small [28]. In contrast, the same-sized battery will not be able to supply the necessary energy in the same time period because of the higher time constant of the battery [27], [29].

The operating voltage of an SC changes linearly with time during constant current operation so that the state-of-charge can be precisely estimated. In addition, the highly reversible electrostatic charge storage mechanism in SCs does not lead to the volume changes observed in batteries with electrochemical transformations of active masses. This volume change usually limits the lifetime cycle of batteries to several hundred cycles, whereas SCs have demonstrated from hundreds of thousands to many millions of full charge/discharge cycles [30], [31].

The SC bank is always connected to the dc bus by means of a two-quadrant dc/dc converter (bidirectional converter). Fig. 2 presents the transient response of an SC converter interfacing between the dc bus and the SC bank (SAFT SC module: 292 F, 30 V) [32]. The initial voltage of the SC bank is 30 V. The SC current set-point (reference) is Ch2 and the measured SC current is Ch4. The dynamic response of the SC auxiliary source is very fast and can discharge from 0 to 50 A in 0.4 ms.

Remark 2: To operate the SC module, its module voltage is limited to an interval $[V_{\text{SCMin}}, V_{\text{SCMax}}]$. The higher V_{SCMax} value of this interval corresponds to the rated voltage of the storage device. In general, the lower V_{SCMin} value is chosen as $V_{\text{SCMax}}/2$, where the remaining energy in the SC bank is only 25% and the SC discharge becomes ineffective [32].

III. SOLAR POWER PLANT

A. Structure of the Studied Power Converters

Low-voltage, high-current (power) converters are needed because of the electrical characteristics of the PV cell and the SC bank. A classical boost converter is often used as a PV converter [33], and a classical two-quadrant (bidirectional) converter is often used as an SC or battery converter [27]. However, the classical converters will be limited when the power increases or at higher step-up ratios. Therefore, the use of parallel power converters (multiphase converters in parallel) with interleaving may offer better performance in terms of dynamics [34], because

IEEE TRANSACTIONS ON ENERGY CONVERSION, VOL. 26, NO. 4, DECEMBER 2011

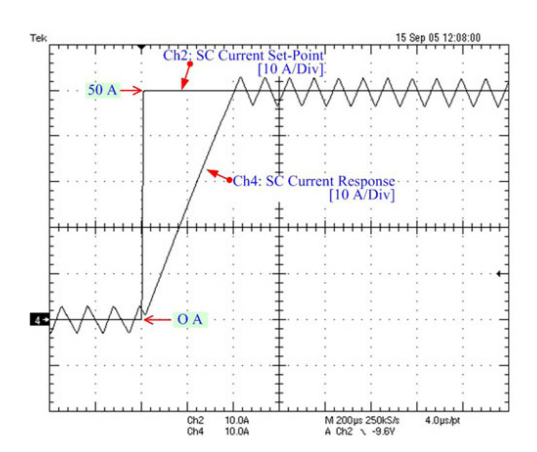


Fig. 2. SC current response to a 0-50 A step (discharging)

1212

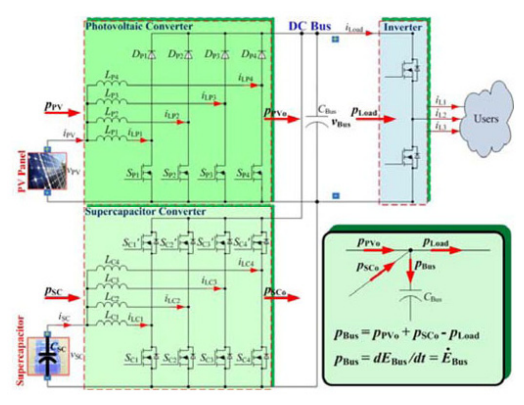


Fig. 3. Proposed circuit diagram of the distributed generation system supplied by a PV and SC, where p_{Load} (= $\nu_{Bus} \times i_{Load}$), ν_{Bus} , and i_{Load} are the load power, the do-bus voltage, and the do-bus load current, respectively, p_{PV} (= $\nu_{PV} \times i_{PV}$), ν_{PV} , and ipv are the PV power, voltage, and current, respectively, p_{SC} (= $\nu_{SC} \times i_{SC}$), ν_{SC} , and i_{SC} are the SC power, voltage, and current, respectively. p_{PVo} and p_{SCo} are the output powers to the do link from the converters of the PV array and the SC, respectively.

of smaller inductor and capacitor sizes. Next, Fig. 3 depicts the proposed hybrid source structure. The PV converter combines four-phase parallel boost converters with interleaving, and the SC converter employs four-phase parallel bidirectional converters with interleaving.

B. Power Regulation Loops of the Proposed Power Plant

For safety and dynamics, the PV and SC converters are primarily controlled by inner current regulation loops (or power regulation loops), as depicted in Figs. 4 and 5 [32]. These power control loops are supplied by two reference signals: the SC power reference p_{SCREF} and the PV power reference p_{PVREF} , generated by the control laws presented later.

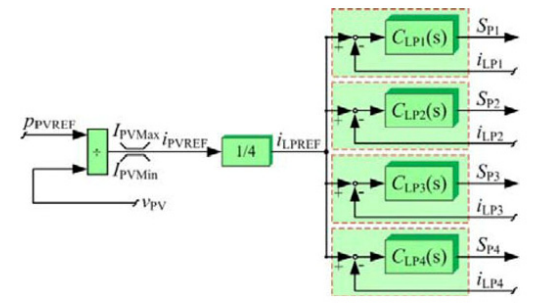


Fig. 4. Photovoltaic power control loop

For the PV power control, a PV power reference p_{PVREF} is divided by the measured photovoltaic voltage v_{PV} , resulting in a PV current reference i_{PVREF} . For the SC power control loop, an SC power reference $p_{\mathtt{SCREF}}$ is divided by the measured SC voltage v_{SC} and limited to maintain the SC voltage within an interval $[V_{\text{SCMin}}, V_{\text{SCMax}}]$, according to Remark 2 by the SC current limitation function. This calculation results in an SC current reference i_{SCREF} [32].

C. Mathematical Model of the Power Plant

We assume that the PV and SC currents follow their reference values perfectly. Consequently,

$$i_{\text{PV}} = i_{\text{PVREF}} = \frac{p_{\text{PV}}}{v_{\text{PV}}} = \frac{p_{\text{PVREF}}}{v_{\text{PV}}}$$
 (1)

$$i_{\text{PV}} = i_{\text{PVREF}} = \frac{p_{\text{PV}}}{v_{\text{PV}}} = \frac{p_{\text{PVREF}}}{v_{\text{PV}}}$$
 (1)
 $i_{\text{SC}} = i_{\text{SCREF}} = \frac{p_{\text{SC}}}{v_{\text{SC}}} = \frac{p_{\text{SCREF}}}{v_{\text{SC}}}.$ (2)

We only consider static losses in these converters, and r_{PV} and r_{SC} represent static losses in the PV and SC converters, respectively. Now, the PV array and the SC storage device function as controlled current sources connected with the equivalent series resistance that is called a reduced-order model [35].

The dc-bus capacitive energy $E_{\mathrm{B}\,\mathrm{us}}$ and the supercapacitive energy E_{SC} can be written as

$$E_{\rm Bus} = \frac{1}{2} C_{\rm Bus} v_{\rm Bus}^2 \tag{3}$$

$$E_{\text{SC}} = \frac{1}{2} C_{\text{SC}} v_{\text{SC}}^2. \tag{4}$$

The total electrostatic energy E_T stored in the dc-bus capacitor C_{Bus} and the SC C_{SC} can also be written as

$$E_T = \frac{1}{2} C_{\text{Bus}} v_{\text{Bus}}^2 + \frac{1}{2} C_{\text{SC}} v_{\text{SC}}^2.$$
 (5)

Note that the total electrostatic energy E_T is nearly equal to the energy stored in the SC $C_{\rm SC}$ because the SC size $C_{\rm SC}$ is much greater than the dc-bus capacitor size C_{Bus} .

The derivative of dc-bus capacitive energy $\dot{E}_{\rm Bus}$ is given versus $p_{\text{PVo}}, p_{\text{SCo}}$, and p_{Load} by the following differential equation:

$$\dot{E}_{\text{Bus}} = p_{\text{PVo}} + p_{\text{SCo}} - p_{\text{Load}} \tag{6}$$

THOUNTHONG: MODEL BASED-ENERGY CONTROL OF A SOLAR POWER PLANT WITH A SUPERCAPACITOR

where

$$p_{\rm PVo} = p_{\rm PV} - r_{\rm PV} \left(\frac{p_{\rm PV}}{v_{\rm PV}}\right)^2 \tag{7}$$

$$p_{SCo} = p_{SC} - r_{SC} \left(\frac{p_{SC}}{v_{SC}}\right)^2 \tag{8}$$

$$p_{Load} = v_{Bus} \cdot i_{Load}$$
 (9)

Note that the derivative of dc-bus capacitive energy $dE_{\rm bus}/dt$ is the power $p_{\rm Bus}$ flows into the dc-bus capacitor. It means that p_{Bus} is equal to dE_{bus}/dt (\dot{E}_{Bus})(see Fig. 3).

IV. CONTROL OF A POWER PLANT

A. Energy Balance

In the proposed system depicted in Fig. 3, there are two voltage variables (or two energy variables) to be regulated.

- The dc-bus energy E_{Bus} is the most important variable.
- 2) The SC storage energy $E_{\rm SC}$ is the next most important.

Therefore, we propose utilizing SCs, which are the fastest energy source in the proposed system, to supply the energy for the dc bus [32]. In fact, we plan to functionalize the PV array by supplying energy only for charging the SC $C_{\rm SC}$. However, during charging, the energy from the PV cell flows through the dc bus to the SC bank. For this reason, the PV array is mathematically operated to supply energy for both the dc-bus capacitor C_{Bus} and the SC C_{SC} to keep them charged.

B. Differential Flatness Property

Let us first reveal a physical property, used to establish the system flatness [14], [15], [36], that will be the main concept for our reference generations. The flat outputs y, the control input variables u, and the state variables x are defined as

$$\mathbf{y} = \begin{bmatrix} y_1 \\ y_2 \end{bmatrix} = \begin{bmatrix} E_{\mathrm{Bus}} \\ E_{\mathrm{T}} \end{bmatrix}, \qquad \mathbf{u} = \begin{bmatrix} u_1 \\ u_2 \end{bmatrix} = \begin{bmatrix} p_{\mathrm{SCREF}} \\ p_{\mathrm{PVDEM}} \end{bmatrix},$$

$$\mathbf{x} = \begin{bmatrix} x_1 \\ x_2 \end{bmatrix} = \begin{bmatrix} v_{\mathrm{Bus}} \\ v_{\mathrm{SC}} \end{bmatrix}$$
(10)

where p_{PVDEM} is the PV power demand. It will be generated by the outer controller. This signal will send to an MPPT in order to saturate the PV maximum power. It becomes the PV power reference p_{PVREF} , presented hereafter.

From (3) and (6), the dc-bus voltage v_{Bus} (defined as a state variable x_1) and the SC power (defined as a control input variable u_1) can be expressed as an algebraic function

$$x_1 = \sqrt{\frac{2y_1}{C_{\text{Bus}}}} = \varphi_1(y_1)$$

$$u_1 = 2p_{\text{SCLim}}$$
(11)

$$\cdot \left[1 - \sqrt{1 - \left(\frac{\dot{y}_1 + i_{\texttt{Load}} \cdot \varphi_1\left(y_1\right) - p_{\texttt{PVo}}}{p_{\texttt{SCLim}}}\right)}\right]$$

$$=\psi_1\left(y_1,\dot{y}_1\right)=p_{\text{SCREF}} \tag{12}$$

$$p_{\text{SCLim}} = \frac{v_{\text{SC}}^2}{4\tau_{\text{SC}}} \tag{13}$$

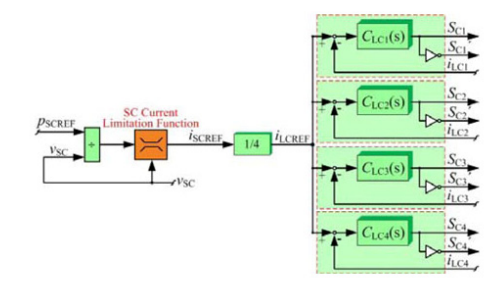


Fig. 5. SC power control loop.

where $p_{\mathtt{SCLim}}$ is the limited maximum power from the SC converter.

From (5) and (6), the SC voltage v_{SC} (defined as a state variable x_2) and the PV power p_{PV} (defined as a control input variable u_2) can be expressed as an algebraic function

$$x_2 = \sqrt{\frac{2(y_2 - y_1)}{C_{SC}}} = \varphi_2(y_1, y_2)$$
 (14)

$$u_{2} = 2p_{\mathrm{PVLim}} \cdot \left[1 - \sqrt{1 - \left(\frac{\dot{y}_{2} + i_{\mathrm{Load}} \cdot \varphi_{1}\left(y_{1}\right)}{p_{\mathrm{PVLim}}}\right)}\right]$$

$$= \psi_2(y_1, \dot{y}_2) = p_{\text{PVDEM}}$$
 (15)

$$p_{\text{PVLim}} = \frac{v_{\text{PV}}^2}{4r_{\text{PV}}}$$
 (16)

where P_{PVLim} is the limited maximum power from the PV converter

It is evident that $x_1 = \varphi_1(y_1), x_2 = \varphi_2(y_1, y_2), u_1 =$ $\psi_1(y_1, \dot{y}_1)$, and $u_2 = \psi_2(y_1, \dot{y}_2)$. Consequently, the PV/SC power plant can be considered a flat system [36].

C. Control Law and Stability

Let us now focus our attention on the feedback design to track a dc-bus energy reference trajectory $y_{1\text{REF}}$ and a total energy reference y_{2 REF}. We aim to design a feedback law such that the tracking error $(y_1 - y_{1REF}, y_2 - y_{2REF})$ asymptotically vanishes. Thus, the relative degree of the first input v_1 and the second input v_2 is 1. The proposed control laws [37] are

$$(\hat{y}_1 - \hat{y}_{1REF}) + K_{11} (y_1 - y_{1REF}) = 0$$
 (17)

$$(\dot{y}_2 - \dot{y}_{2REF}) + K_{21} (y_2 - y_{2REF}) = 0.$$
 (18)

Because the SC can store enormous amount of energy, and the supercapacitive energy is defined as a slower dynamic variable than the dc-bus energy variable, in order to compensate for nonideal effects, an integral term is added to the control law (17). This yields

$$v_{1} = \dot{y}_{1} = \dot{y}_{1RBF} + K_{11} (y_{1RBF} - y_{1})$$

$$+ K_{12} \int_{0}^{t} (y_{1REF} - y_{1}) d\tau$$
(19)

TRF: MRG5380261

IEEE TRANSACTIONS ON ENERGY CONVERSION, VOL. 26, NO. 4, DECEMBER 2011

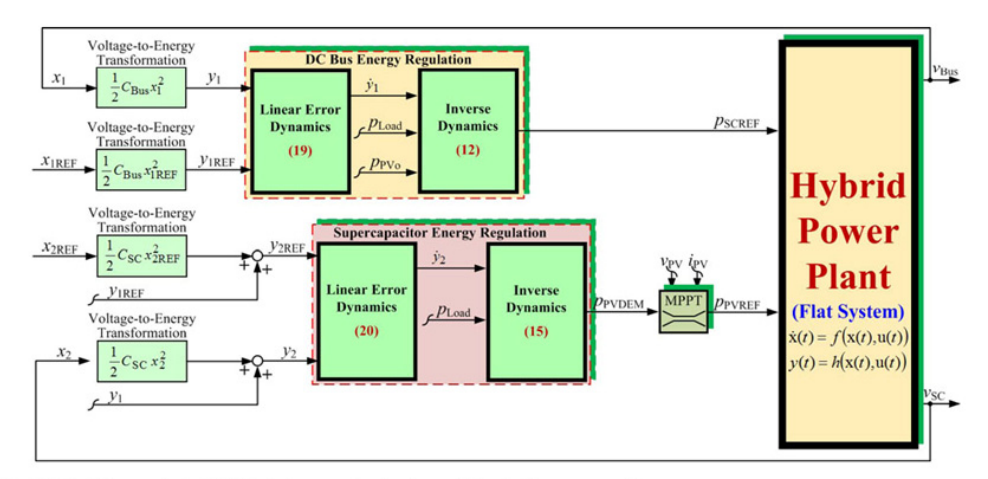


Fig. 6. Multivariable control of a PV/SC hybrid power plant based on a differential flatness approach.

$$v_2 = \dot{y}_2 = \dot{y}_{2REF} + K_{21} (y_{2REF} - y_2).$$
 (20)

From (19), if we define $e_1=y_1-y_{1\rm REP},\,K_{11}=2\zeta\omega_n,$ and $K_{12}=\omega_n^2,$ we obtain

$$\ddot{e}_1 + 2\zeta\omega_n \cdot \dot{e}_1 + \omega_n^2 \cdot e_1 = 0. \tag{21}$$

Substituting the expression for \dot{y}_1 from (19) into (12) gives the equation for the closed-loop static state feedback SC power. From (20), if we define $e_2 = y_2 - y_{2\text{REP}}$, $K_{21} = 1/\tau_S$, we obtain

$$\tau_8 \cdot \dot{e}_2 + e_2 = 0. \tag{22}$$

Substituting the expression for \dot{y}_2 from (20) into (15) gives the equation for the closed-loop static state feedback PV power. It is clear that the control system is asymptotically stable for K_{11} , $K_{12}>0$, and $K_{21}>0$. However, based on the power electronic constant switching frequency $\omega_{\mathcal{S}}$ and cascade control structure, the outer control loop (here the dc-bus energy control) must operate at a cutoff frequency $\omega_{\mathcal{E}}<<\omega_{\mathcal{C}}<<\omega_{\mathcal{S}}$, where $\omega_{\mathcal{C}}$ is a cutoff frequency of the SC power loop. Once the flat outputs are stabilized, the whole system becomes exponentially stable because all of the variables of the system are expressed in terms of the flat outputs [36].

In Fig. 6, the proposed control algorithm of the renewable energy power plant, as detailed earlier, is depicted. The dc-bus energy control law generates an SC power reference $p_{\rm SCREF}$ (= u_1 , refer to (12)). The total energy control law (or the SC energy control) generates a PV power demand $p_{\rm PVDEM}$ (= u_2 , refer to (15)). This signal must be saturated at the maximum power point by MPPT according to *Remark 1*.

It should be concluded here that, in this application, the PV does not always operate at its MPP in a stand-alone (grid-independent) scenario, as depicted in Fig. 6.

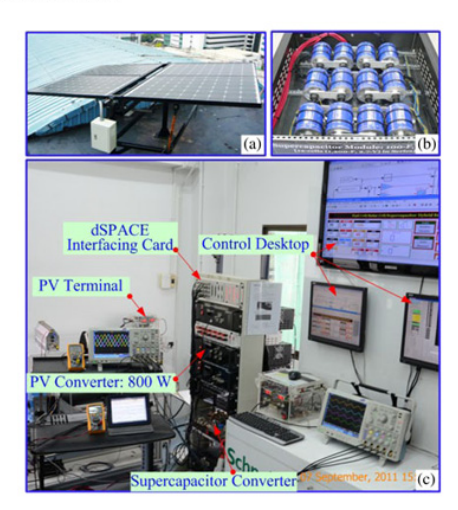


Fig. 7. Photograph of a test bench power plant. (a) solar cell panels, (b) SC bank, and (c) test bench.

V. PERFORMANCE VALIDATIONS

A. Power Plant Description for a Test Bench

To validate the performance of the modeling and control system, the small-scale test bench of the hybrid power plant was implemented in our laboratory, as presented in Fig. 7. The prototype 0.8-kW PV converter and the 2-kW SC converter (refer to Fig. 3) were implemented in the laboratory. Specifications of the PV module and storage device are detailed in Table I.

 $\label{eq:TABLEI} \mbox{TABLE I}$ Specifications of Photovoltaic Source and Storage Device

Photovoltaic Array (by Ekarat Solar Co	mpany):	
Number of Panels in Parallel	4	
Panel Open Circuit Voltage	33.5	V
Panel Rated Voltage	26	V
Panel Rated Current	7.7	A
Panel Rated Power	200	W
Array Rated Power	800	W
Supercapacitor Bank (by Maxwell Tec	hnologies	Comp
(Cell Model: BCAP1200)		
Number of Cells in Series	12	
Cell Capacity	1,200	F
Cell Maximum Voltage	2.7	V
Bank Capacity (C _{SC})	100	F
Bank Maximum Voltage	32	V

TABLE II DC-Bus Energy Control Loop Parameters

v_{BusREF}	60	V	
C_{Bus}	12200	μ F	
K_{11}	450	rad·s-1	
K_{12}	22,500	rad2·s-2	
$r_{\rm PV}$	0.12	Ω	
$r_{\rm SC}$	0.10	Ω	
V_{SCMax}	32	V	
$V_{\rm SCMin}$	15	V	
I_{SCRated}	150	A	

TABLE III
SUPERCAPACITIVE ENERGY CONTROL LOOP PARAMETERS

VSCREF	25	V	
C_{SC}	100	F	
K_{21}	0.1	$W \cdot J^{-1}$	
p _{PVMax} (Rated)	800	W	
I _{PVMax} (Rated)	30.8	A	
I_{PVMin}	0	A	
ΔI_{PV}	0.1	A	
Δt	6	ms	

B. Control Description

The parameters associated with the dc-bus energy regulation loop are summarized in Table II. The parameters associated with the SC energy regulation loop are detailed in Table III. For the low-scale test bench, the dc-bus voltage reference $v_{\rm BusREF}$ (= $x_{\rm 1REF}$) was set to 60 V and the SC voltage reference $v_{\rm SCREF}$ (= $x_{\rm 2REF}$) was set to 25 V (the nominal value of the SC bank).

The constant switching frequency ω_S of the PV and SC converters was 25 kHz (157 080 rad·s⁻¹). The nonlinear controller gains used were $K_{11}=450~{\rm rad\cdot s^{-1}}$ and $K_{12}=22~500~{\rm rad^2\cdot s^{-2}}$ so that the system damping ratio ζ was equal to 1.5 and the natural frequency ω_R was equal to 150 rad·s⁻¹. As a result, the cutoff frequency ω_E of the closed-loop dc-bus energy was equal to 60 rad·s⁻¹. This value was lower than the cutoff frequency ω_C of the SC power loop of 450 rad·s⁻¹ (equivalent to a first-order delay with a time constant T_C of 2.2 ms) so that the system was asymptotically stable [36]. The controller gain of the closed-loop supercapacitive energy was $K_{21}=0.1~{\rm W\cdot J^{-1}}$ so that the cutoff frequency ω_{SC} of the closed-loop supercapacitive

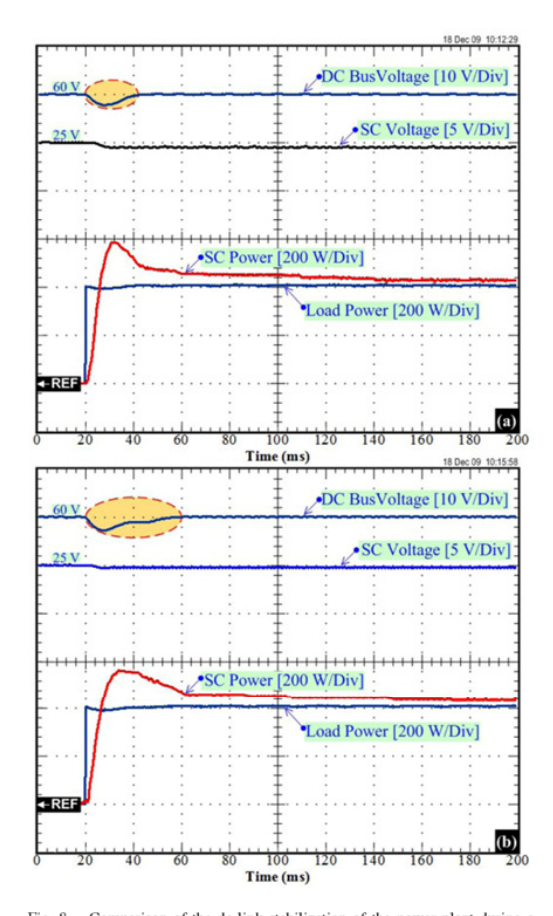


Fig. 8. Comparison of the dc-link stabilization of the power plant during a large load step. (a) Exact model ($r_{\rm PV}=0.12~\Omega, r_{\rm SC}=0.10~\Omega$). (b) Error model (robustness) ($r_{\rm PV}=0.001~\Omega, r_{\rm SC}=0.001~\Omega$).

energy was equal to 0.1 rad·s $^{-1}$ in which $\omega_{SC}<<\omega_{E},$ in order to guarantee the asymptotic stability of the whole system.

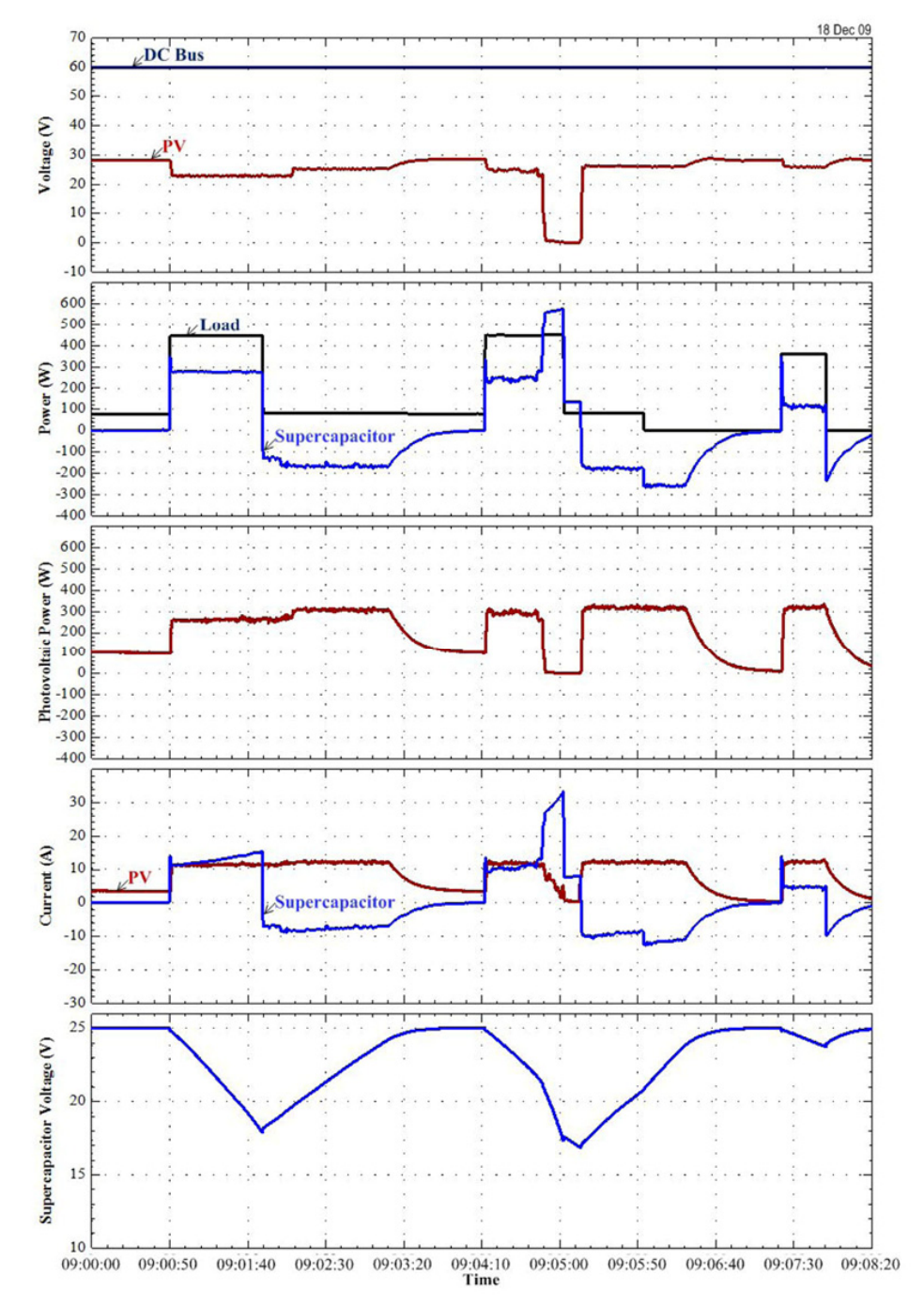
The PV and SC current regulation loops and the electronic protections were realized by analog circuits. The two energy-control loops, which generate current references i_{PVREF} and i_{SCREF} , were implemented in the real-time card dSPACE DS1104 platform (see Fig. 7) using the fourth-order *Runge–Kutta* integration algorithm and a sampling time of 80 μ s within the mathematical environment of MATLAB—Simulink.

C. Experimental Results

Because flatness-based control is model based, it may have some sensitivity to error in model parameters. To authenticate its robustness, the flatness-based control was tested with the exact model parameters ($r_{\rm PV}=0.12~\Omega$ and $r_{\rm SC}=0.10~\Omega)$ and the erroneous parameters case ($r_{\rm PV}=0.001~\Omega$ and $r_{\rm SC}=$

IEEE TRANSACTIONS ON ENERGY CONVERSION, VOL. 26, NO. 4, DECEMBER 2011





 $Fig.\,9.\quad Experimental\ results:\ power\ plant\ response\ during\ load\ cycles.$

 $0.001\,\Omega$). For the sake of the dc-bus voltage stabilization and robust control system, the oscilloscope waveforms in Fig. 8 show the comparison (robustness) between the accurate parameters and the error parameters. It portrays the dynamic characteristics that are obtained during the large load step. It shows the dc-bus voltage, the load power (disturbance), the SC power, and the SC voltage. The initial state is in no-load power, the SC storage device is full of charge, i.e., the SC voltage = 25 V (VSCREF = 25 V), and the dc-bus voltage is regulated at 60 V ($\nu_{\rm BusREF}$ = 60 V); as a result, the PV and SC powers are zero. At t =20 ms, the large load power steps from 0 W to a constant value of 400 W (positive transition). Because during the transient state the PV power is limited by MPPT estimation, the SC supplies the transient load power demand. One can scrutinize the similar waveforms in Fig. 8(a) and (b). The dc-bus voltage (dc-link stabilization) is minimally influenced by the large load power step. Clearly, the performance of the control system is minimally affected by the model parameter error considered. Experimental testing demonstrates that errors in these parameters had relatively little effect on regulation performance, and we conclude that the nonlinear differential flatness-based approach provides a robust controller in this application.

Finally, for the sake of the dc-bus voltage stabilization and load profile (load cycles), Fig. 9 presents waveforms that are obtained during the load cycles measured on December 18, 2009, at an ambient temperature of around 25 °C. In Fig. 9, the dc-bus voltage, the PV voltage, the load power (disturbance), the SC power, the PV power, the SC current, the PV current, and the SC voltage are shown. In the initial state, the small load power is equal to 100 W, and the storage device is full of charge, i.e., $\nu_{\rm SC}=25$ V; as a result, the SC power is zero and the PV source supplies 100 W of power for the load. At 09:00:50, the load power steps to the final constant power of around 450 W (positive load power transition). We observe the following phenomena.

- The SC supplies most of the transient power that is required during the step load.
- Simultaneously, the PV power increases to an MPP of around 250 W, which is limited by the MPPT.
- Concurrently, the SC remains in a discharge state after the load step because the steady-state load power (approximately 450 W) is greater than the power supplied by the PV array.

After that phase, one can again observe that the power plant is always energy balanced $(p_{\text{Load}}(t) = p_{\text{PV}}(t) + p_{\text{SC}}(t))$ by the proposed original control algorithm. One can observe that the dc-bus voltage waveform is asymptotically stable during the large load cycles, which is of major importance when employing SC to improve the dynamic performance of the whole system using the proposed control law.

VI. CONCLUSION AND FURTHER WORKS

The main contribution of this paper is to model and control a PV/SC hybrid power plant. The prototype power plant is composed of a PV array (800 W, Ekarat Solar) and an SC module (100 F, 32 V, Maxwell Technologies). A compact topology,

suitable for high-power applications, is proposed. Its working principle, analysis, and design procedure are presented. The PV array is the main source, and the SC functions as a storage device (or an auxiliary source) to compensate for the uncertainties of the PV source in the steady state and the transient state. An SC can advance the load, following the characteristics of the main sources, by providing a stronger power response to changes in the system load. Adding energy storage to the distributed power systems improves power quality and efficiency.

Using the nonlinear control approach based on the flatness property, we propose a simple solution to the dynamic, stabilization, and robustness problems in the nonlinear power electronic system. And also, there are no operating points comparable with a classical linear control. This is a novel concept for this kind of application. However, the proposed control law needs a load current measurement to estimate the load power. For future work, a load observer will be used to avoid a measurement of a load current, as was explored in [23].

ACKNOWLEDGMENT

The author would like to thank Dr. P. Sethakul (KMUTNB), Dr. S. Pierfederici, and Dr. B. Davat (Nancy University) for their valuable comments and suggestions about power electronics and control.

REFERENCES

- Y. Cheng, "Assessments of energy capacity and energy losses of supercapacitors in fast charging–discharging cycles," *IEEE Trans. Energy Convers.*, vol. 25, no. 1, pp. 253–261, Mar. 2010.
 M. Liserre, T. Sauter, and J. Y. Hung, "Future energy systems: Integrating
- [2] M. Liserre, T. Sauter, and J. Y. Hung, "Future energy systems: Integrating renewable energy sources into the smart power grid through industrial electronics," *IEEE Ind. Electron. Mag.*, vol. 4, no. 1, pp. 18–37, Mar. 2010.
- [3] A. El Aroudi and M. Orabi, "Stabilizing technique for AC-DC boost PFC converter based on time delay feedback." *IEEE Trans. Circuits Syst. II, Exp. Briefs*, vol. 57, no. 1, pp. 56-60, Jan. 2010.
 [4] Suroso and T. Noguchi, "A new three-level current-source PWM inverter
- [4] Suroso and I. Noguch, "A new three-level current-source PWM inverter and its application for grid connected power conditioner," *Energy Con*vers. Manage., vol. 51, no. 7, pp. 1491–1499, Jul. 2010.
- Y.A. Hajizadeh, M. A. Golkar, and A. Feliachi, "Voltage control and active power management of hybrid fuel-cell/energy-storage power conversion system under unbalanced voltage sag conditions," *IEEE Trans. Energy Convers.*, vol. 25, no. 4, pp. 1195–1208, Dec. 2010.
 L. Ming, C. K. Tse, H. H. C. Iu, M. Xikui, and M. Orabi, "Unified
- [6] L. Ming, C. K. Tse, H. H. C. Iu, M. Xikui, and M. Orabi, "Unified equivalent modeling for stability analysis of parallel-connected DC/DC converters," *IEEE Trans. Circuits Syst. II, Exp. Briefs*, vol. 57, no. 11, pp. 898–902, Nov. 2010.
- [7] P. Thounthong, S. Pierfederici, J.-P. Martin, M. Hinaje, and B. Davat, "Modeling and control of fuel cell/supercapacitor hybrid source based on differential flatness control," *IEEE Trans. Veh. Technol.*, vol. 59, no. 6, pp. 2700–2710, Jul. 2010.
 [8] N. Gyawali and V. O.
- [8] N. Gyawali and Y. Ohsawa, "Integrating fuel cell/electrolyzer/ultracapacitor system into a stand-alone microhydro plant," *IEEE Trans. Energy Convers.*, vol. 25, no. 4, pp. 1092–1101, Dec. 2010.
- K. Acharya, S. K. Mazumder, and I. Basu, "Reaching criterion of a three-phase voltage source inverter operating with passive and nonlinear loads and its impact on global stability," *IEEE Trans. Ind. Electron.*, vol. 55, no. 4, pp. 1795–1812, Apr. 2008.
 X. Yu and O. Kaynak, "Sliding-mode control with soft computing: A
- [10] X. Yu and O. Kaynak, "Sliding-mode control with soft computing: A survey," *IEEE Trans. Ind. Electron.*, vol. 56, no. 9, pp. 3275–3285, Sep. 2009.
 [11] W. K. Na and B. Gou, "Feedback-linearization-based nonlinear control for
- [11] W. K. Na and B. Gou, "Feedback-linearization-based nonlinear control for PEM fuel cells," *IEEE Trans. Energy Convers.*, vol. 23, no. 1, pp. 179– 190, Mar. 2008.

- F. Jadot, F. Malrait, J. Moreno-Valenzuela, and R. Sepulchre, "Adaptive regulation of vector-controlled induction motors," *IEEE Trans. Control Syst. Technol.*, vol. 17, no. 3, pp. 646–657, May 2009.
 C.-S. Chiu, "T-S fuzzy maximum power point tracking control of solar
- [13] C.-S. Chiu, "1-S fuzzy maximum power point tracking control of solar power generation systems," *IEEE Trans. Energy Convers.*, vol. 25, no. 4, pp. 1123–1132, Dec. 2010.
 [14] M. Fliess, J. Lévine, Ph. Martin, and P. Rouchon, "Flatness and defect of nonlinear systems: Introductory theory and examples," *Int. J. Contr.*, vol. 41, pp. 4123–4232, 1326, 1327.
- vol. 61, no. 6, pp. 1327–1361, 1995. [15] M. Fliess, J. Lévine, Ph. Martin, and P. Rouchon, "A Lie-Bäcklund approach to equivalence and flatness of nonlinear systems," *IEEE Trans.*
- proach to equivalence and flatness of nonlinear systems," *IEEE Trans. Automat. Contr.*, vol. 44, no. 5, pp. 922–937, May 1999.
 [16] M. Guay, "On the linearizability of nonisothermal continuous stirred-tank reactors," *Automatica*, vol. 38, no. 2, pp. 269–278, Feb. 2002.
 [17] J. Villagra, B. A. Novel, H. Mounier, and M. Pengov, "Flatness-based vehicle steering control strategy with SDRE feedback gains tuned via a sensitivity approach," *IEEE Trans. Control Syst. Technol.*, vol. 15, no. 3, pp. 554–564, May 2007.
- [18] H. Aschemann and D. Schindele, "Sliding-mode control of a high-speed linear axis driven by pneumatic muscle actuators," *IEEE Trans. Ind. Electron.*, vol. 55, no. 1, pp. 3855–3864, Nov. 2008.
 [19] M. A. Danzer, J. Wilhelm, H. Aschemann, and E. P. Hofer, "Model-based
- control of cathode pressure and oxygen excess ratio of a PEM fuel cell system," *J. Power Sources*, vol. 176, no. 2, pp. 515–522, Feb. 2008.

 [20] P. S. P. da Silva and P. Rouchon, "Flatness-based control of a single qubit
- gate,," IEEE Trans. Automat. Contr., vol. 53, no. 3, pp. 775-779, Apr.
- [21] E. Song, A. F. Lynch, and V. Dinavahi, "Experimental validation of nonlinear control for a voltage source converter," *IEEE Trans. Control Syst. Technol.*, vol. 17, no. 5, pp. 1135–1144, Sep. 2009.
- Technol., vol. 17, no. 3, pp. 1132–1144, ps. 2, 2009.

 T. Rabbani, S. Munier, D. Dorchies, P. Malaterre, A. Bayen, and X. Litrico, "Flatness-based control of open-channel flow in an irrigation canal using SCADA," *IEEE Control Syst. Mag.*, vol. 29, no. 5, pp. 22–30, Oct. 2009.

 A. Gensior, H. Sira-Ramirez, J. Rudolph, and H. Guldner, "On some non-linear current controllers for three-phase boost rectifiers,," *IEEE Trans.*

- linear current controllers for three-phase boost rectifiers,," IEEE Trans. Ind. Electron., vol. 56, no. 2, pp. 360–370, Feb. 2009.

 [24] L. R. Chen, C. H. Tsai, Y. L. Lin, and Y. S. Lai, "A biological swarm chasing algorithm for tracking the PV maximum power point," IEEE Trans. Energy Convers., vol. 25, no. 2, pp. 484–493, Jun. 2010.

 [25] T. L. Gibson and N. A. Kelly, "Solar photovoltaic charging of lithium-ion batteries," J. Power Sources, vol. 195, no. 12, pp. 3928–3932, Jun. 2010.

 [26] O. Lopez, F. D. Freijedo, A. G. Yepes, P. F. Comesana, J. Malvar, R. Teodorescu, and J. Doval-Gandoy, "Eliminating ground current in a transformerless photovoltaic application," IEEE Trans. Energy Convers., vol. 25, no. 1, pp. 140–147, Mar. 2010.

 [27] A. Khaligh and Z. Li, "Battery, ultracapacitor, fuel cell, and plug-in hybrid electric vehicles: state of the art," IEEE Trans. Veh. Technol., vol. 59.
- electric vehicles: state of the art," IEEE Trans. Veh. Technol.. vol. 59. no. 6, pp. 2806–2814, Jul. 2010.

 [28] J. R. Mille, "Introduction to electrochemical capacitor technology," *IEEE*
- Electr. Insulat. Mag. Mille, vol. 26, no. 4, pp. 40-47, Jul. 2010

- [29] V. Agarwal, K. Uthaichana, R. A. DeCarlo, and L. H. Tsoukalas, "Dev. Agarwai, K. Omatchana, K. A. DeCarlo, and L. H. Isoukalas, Development and validation of a battery model useful for discharging and charging power control and lifetime estimation," *IEEE Trans. Energy Convers.*, vol. 25, no. 1, pp. 140–147, Mar. 2010.
 M. Inagaki, H. Konno, and O. Tanaike, "Carbon materials for electrochemical capacitors," *J. Power Sources*, vol. 195, no. 24, pp. 7880–7903,
- Dec. 2010.
- A. Hammar, P. Venet, R. Lallemand, G. Coquery, and G. Rojat, " of accelerated aging of supercapacitors for transport applications," *IEEE Trans. Ind. Electron.*, vol. 57, no. 12, pp. 3972–3979, Dec. 2010.
 P. Thounthong, S. Raël, and B. Davat, "Analysis of supercapacitor as
- P. Thounthong, S. Raël, and B. Davat, "Analysis of supercapacitor as second source based on fuel cell power generation," *IEEE Trans. Energy Convers.*, vol. 24, no. 1, pp. 247–255, Mar. 2009.

 G. Spagnuolo, G. Petrone, S. V. Araujo, C. Cecati, E. Friis-Madsen, E. Gubia, D. Hissel, M. Jasinski, W. Knapp, M. Liserre, P. Rodriguez, R. Teodorescu, and P. Zacharias, "Renewable energy operation and conversion schemes: A summary of discussions during the seminar on renewable energy systems," in *IEEE Ind. Electron. Mag.*, no. 1. vol. 4, Mar. 2010, pp. 38–51.

 P. Thounthone and D. Deney (1997).
- pp. 36-31.
 [34] P. Thounthong and B. Davat, "Study of a multiphase interleaved stepup converter for fuel cell high power applications,," Energy Convers.

 Manage., vol. 51, no. 4, pp. 826–832, Apr. 2010.

 S. D. Sudhoff, K. A. Corzine, S. F. Glover, H. J. Hegner, and H. N. Robey,
- Jr., "DC link stabilized field oriented control of electric propulsion systems," *IEEE Trans. Energy Convers*, vol. 13, no. 1, pp. 27–33, Mar. 1998.
- P. Thounthong, S. Pierfederici, and B. Davat, "Analysis of differential flatness-based control for a fuel cell hybrid power source," IEEE Trans. Energy Convers., vol. 25, no. 3, pp. 909–920, Sep. 2010. P. Thounthong and S. Pierfederici, "A new control law based on the dif-
- ferential flatness principle for multiphase interleaved DC–DC converter," IEEE Trans. Circuits Syst. II, Exp. Briefs, vol. 57, no. 11, pp. 903–907, Nov. 2010.



Phatiphat Thounthong (M'09) received the B.S. Phatiphat Thounthong (M 09) received the B.S. and M.E. degrees in electrical engineering from King Mongkut's Institute of Technology North Bangkok (KMITNB), Bangkok, Thailand, in 1996 and 2001, respectively, and the Ph.D. degree in electrical engineering the Marian Phatiphan (Marian Panalan) and the Ph.D. degree in electrical engineering the Marian Phatiphan (Marian Phatiphan) and the Ph.D. degree in electrical engineering the Marian Phatiphan (Marian Phatiphan) and Marian (Marian neering from the Institut National Polytechnique de Lorraine (INPL)-Nancy University, Nancy-Lorraine, France, in 2005.

He is currently an Associate Professor in the De-partment of Teacher Training in Electrical Engineer-

ing (TE), King Mongkut's University of Technology North Bangkok (KMUTNB). His current research interests include power electronics, electric drives, and electrical devices (fuel cell, solar cell, wind turbine, batteries, and SC).

IEEE TRANSACTIONS ON CIRCUITS AND SYSTEMS—II: EXPRESS BRIEFS, VOL. 57, NO. 11, NOVEMBER 2010

903

A New Control Law Based on the Differential Flatness Principle for Multiphase Interleaved DC-DC Converter

Phatiphat Thounthong, Member, IEEE, and Serge Pierfederici

Abstract-This brief presents an innovative control law for a distributed de generation supplied by a de power source, here, a fuel cell (FC) generator. Basically, an FC is always connected with a power-electronic converter. This kind of system is a nonlinear behavior. Classically, to control the voltage, the current, or the power in the converter, a linearized technique is often used to study the stability and to select the controller parameters of the nonlinear converter. In this brief, a nonlinear-control algorithm based on the flatness property of the system is proposed. Flatness provides a convenient framework for meeting a number of performance specifications on the power converter. Utilizing the flatness property, we propose simple solutions to the system performance and stabilization problems. Design controller parameters are autonomous of the operating point. To validate the proposed method, a prototype FC power converter (1.2-kW four-phase boost converters in parallel) is realized in the laboratory. The proposed control law based on the flatness property is implemented by digital estimation in a dSPACE 1104 controller card. Experimental results with a polymer electrolyte membrane FC of 1200 W and 46 A in the laboratory corroborate the excellent control scheme.

Index Terms-Converters, flatness-based control, fuel cells (FCs), interleaved, nonlinear, power control.

I. INTRODUCTION

POLYMER electrolyte membrane fuel cells (PEMFCs) as de generators have become an overwhelming competitor in the distributed generation due to their insuperable advantages, such as high energy efficiency, near-zero emissions, case of installation, quiet operation, and fewer moving parts and higher power quality [1], [2].

Manuscript received March 8, 2010; revised May 10, 2010 and July 2, 2010; accepted August 23, 2010. Date of publication November 1, 2010; date of current version November 17, 2010. This work was supported in part by a research program in cooperation with the Thai-French Innovation Institute, King Mongkut's University of Technology North Bangkok (KMUTNB), and the Institut National Polytechnique de Lorraine, Nancy Université, under the Franco-Thai Higher Education and Research Joint Project (2009-2010), by the Faculty of Technical Education under Grant FTE255301, by the Thailand Research Fund under Grant MRG5380261, by the National Research Council of Thailand under Grant NRCT40/2553, and by KMU/INB under Grant KMUTNB2553. This paper was recommended by Associate Editor H. S.-H. Chung.

H. S.-H. Chung.
P. Thounthong is with the Department of Teacher Training in Electrical Engineering and the Renewable Emergy Research Centre, King Mongkut's University of Technology North Bangkok, Bangkok 10800. Thailand (e-mail: pht@kmutho ac.th; Phatiphat Thounthong@ensem.inpl-nancyfe).
S. Pierfederici is with the Groupe de Recherche en Electrotechnique et Electronique de Nancy, Institut National Polytechnique de Loraine, Nancy Université. 54510 Nancy, France (e-mail: Serge.Pierfedecic@ensem.inpl-nancyfr).
Digital Object Identifier 10.1109/TCSIL2019.2082830

Parallel de-de converters are widely used in high-power applications [2]. They operate under a closed-loop feedback control to regulate the output voltage and enable load sharing. These closed-loop converters are intrinsically nonlinear systems. The common method of controlling do-do chopper converters still relies on averaged small-signal models and then facilitating the application of the linear-control theory, such as the proportional-integral (PI) controller [3]. Nonetheless, there are situations where this technique offers a limited performance.

This brief presents a new control law based on the differential flatness theory for nonlinear power-electronic switching applications. Here, only the inner fuel cell (FC) power regulation loop is studied. In this kind of system, the main important specification is that a power dynamic response must follow a power reference as fast as possible. By using the nonlinear flatness property, the power regulation loop will operate at very high dynamics. This brief is organized as follows. Section II shows the differential equations describing the ideal multiphase boost converters with an interleaving switching technique for FC high-power applications. In Section III, the brief of the differential flatness principle is introduced. Section IV discusses the proof of differential flatness of the proposed FC converter models and the control law and stability. Experimental results will authenticate the proposed control system in Section V. A comparative study between the flatness control and a linear PI control will be presented in Section VI. Finally, this brief ends with concluding remarks in Section VII.

II. MULTIPHASE INTERLEAVED BOOST CONVERTER FOR FC HIGH-POWER APPLICATIONS

A. Power Converter

Fundamentally, low-voltage high-current (power) converters are needed because of the FC electrical characteristics [1]. A classical boost converter is frequently selected as an FC converter [2], [4]. However, the classical converters will be limited when the power increases or for higher step-up ratios. In this manner, the utilization of parafleling power converters (multiphase converter in parallel) with an interleaved technique may offer some better performances [2]. As a general rule, the interleaved switching technique is composed of phase shifting the control signals of several converter cells N in parallel [5]. Fig. 1 shows the functional diagram of the proposed multiphase interleaved step-up converter for FC applications.

1549-7747/\$26.00 © 2010 IEEE

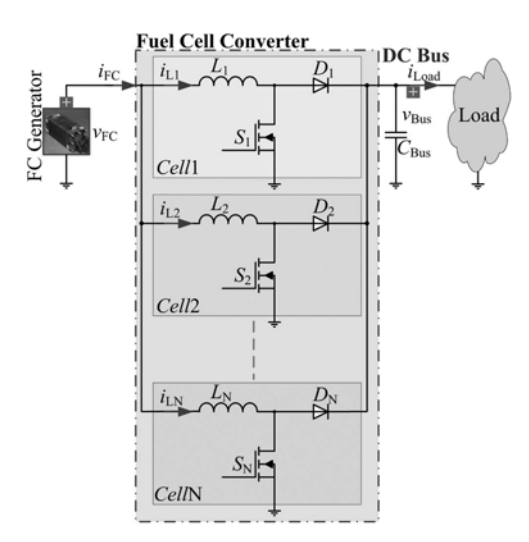


Fig. 1. Multiphase parallel boost converters for FC applications.

B. Boost Converter Average Model

904

The state equations of the multiphase converters are given as

$$L_K \frac{di_{L_K}}{dt} = v_{FC} - R_{L_K} \cdot i_{L_K} - (1 - d_K) \cdot v_{Bus} \quad (1)$$

$$C_{\text{Bus}} \frac{dv_{\text{Bus}}}{dt} = \sum_{K=1}^{N} (1 - d_K) \cdot i_{L_K} - \frac{v_{\text{Bus}}}{R_{\text{Load}}}$$
(2)

where the subscript number K = 1, 2, ..., N represents the parameters of each converter module, d is the duty cycle of the pulsewidth modulation (PWM) converter, v_{Bus} is the dc bus voltage, v_{FC} is the FC voltage, i_{FC} is the FC current, i_L is the inductor current, $R_{\rm Load}$ is the equivalent resistance as a load at the dc bus, L is the input inductance, C_{Bus} is the total output capacitance at the dc bus, and R_L is the series resistance of inductor ${\cal L}_K.$ Note that ${\cal R}_L$ represents the static losses in each boost converter module.

The power of each cell can be written as

$$p_{L_1} = v_{\text{FC}} \cdot i_{L_1}, p_{L_2} = v_{\text{FC}} \cdot i_{L_2}, \dots, p_{L_N} = v_{\text{FC}} \cdot i_{L_N}$$
 (3)

$$p_{\rm FC} = \sum_{i=1}^{N} v_{\rm FC} \cdot i_{L_K} \tag{4}$$

$$p_{\rm FC} = v_{\rm FC} \cdot i_{\rm FC}. \tag{5}$$

Then, the input power p_L of each cell is given versus v_{FC} and i_L by the following differential equation:

$$\frac{dp_L}{dt} = \frac{d(v_{FC} \cdot i_L)}{dt} = i_L \cdot \frac{dv_{FC}}{dt} + v_{FC} \cdot \frac{di_L}{dt}$$
(6)

$$\frac{dp_L}{dt} = v_{FC} \cdot \frac{di_L}{dt} \Big|_{v_{FC} = Constant}.$$
(7)

III. BRIEF OF THE DIFFERENTIAL FLATNESS PRINCIPLE

Currently, many modeling and linear- or nonlinear-control methods, including classical state-space or transfer approaches [6], self-tuning methods or sliding mode control [7], or fuzzy-

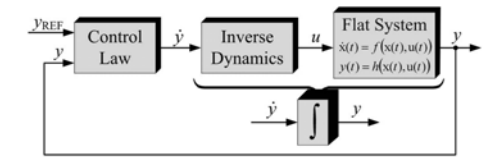


Fig. 2. Concept of the flatness-based control, where y is the output variable, $y_{\rm REF}$ is the output setpoint, and u is the control input variable

logic-based control [8], [9], have been extensively studied for nonlinear power-electronic applications.

The flatness theory was introduced by Fliess et al. [10] in 1995. Lately, these ideas have been used in a variety of nonlinear systems across the various engineering disciplines, including the following: the control of an inverted pendulum and a vertical takeoff and landing aircraft [10]; the control of cathode pressure and oxygen excess ratio of a PEMFC system [11]; the reactive power and dc voltage tracking control of a three-phase voltage source converter [12]; and the current control for three-phase three-wire boost converters [13]. Since the flatness-based control is model based, one expects it to have some sensitivity to error in model parameters. However, Song et al. [12] have proved that the flatness-based control is robust and provides an improved transient tracking performance relative to a traditional linear-control (PI controller) method.

A nonlinear system is flat [9], [14], [15] if there exists a set of differentially independent variables (equal in number to the number of inputs) such that all state variables x and (control) input variables u can be expressed in terms of those output variables y and a finite number of their time derivatives without integrating differential equations. More specifically, consider the nonlinear dynamic system of the general form, i.e.

$$\begin{aligned}
\dot{\mathbf{x}}(t) &= f\left(\mathbf{x}(t), \mathbf{u}(t)\right) \\
\mathbf{y}(t) &= h\left(\mathbf{x}(t), \mathbf{u}(t)\right)
\end{aligned} (8)$$

where

$$\mathbf{x} = [x_1, x_2, \dots x_n]^T, \quad \mathbf{x} \in \Re^n$$
 (9)

$$\mathbf{x} = [x_1, x_2, \dots x_n]^T, \qquad \mathbf{x} \in \Re^n \qquad (9)$$

$$\mathbf{u} = [u_1, u_2, \dots u_m]^T, \qquad \mathbf{u} \in \Re^m \qquad (10)$$

$$\mathbf{y} = [y_1, y_2, \dots, y_m]^T, \qquad \mathbf{y} \in \Re^m \qquad (11)$$

$$\mathbf{y} = [y_1, y_2, \dots, y_m]^T, \qquad \mathbf{y} \in \Re^m \tag{11}$$

 $f(\cdot)$ and $h(\cdot)$ are smooth nonlinear functions, and $(n, m) \in \mathbb{N}$. Moreover, it is assumed that $m \leq n$.

As depicted in Fig. 2, the nonlinear flat systems are equivalent to the linear controllable systems. A system is denoted flat if an output vector y exists, which fulfills the following conditions:

The output variables y_i can be stated as functions of the state variables x_i , the input variables u_i , and a finite number α of their time derivatives, i.e.

$$\mathbf{y} = \phi\left(\mathbf{x}, u, \dot{u}, \dots, u^{(\alpha)}\right).$$
 (12)

2) All state variables x_i and all control inputs u_i can be stated as functions of the output variables y_i and a finite number β of their time derivatives, i.e.

$$\mathbf{x} = \varphi \left(y, \dot{y}, \dots, y^{(\beta)} \right)$$

$$\mathbf{u} = \psi \left(y, \dot{y}, \dots, y^{(\beta+1)} \right)$$
(13)

$$\mathbf{u} = \psi\left(y, \dot{y}, \dots, y^{(\beta+1)}\right) \tag{14}$$

where $\phi(\cdot)$, $\varphi(\cdot)$, and $\psi(\cdot)$ are smooth mapping functions.

If the output variables of interest can be proven to be flat outputs y, the reference signal $y_{\rm REF}$ becomes straightforward.

IV. POWER CONTROL LOOP OF THE MULTIPHASE INTERLEAVED BOOST CONVERTER

A. Flatness of the Boost Converter

Controlling an interleaved multiphase converter is the same as controlling a single boost converter, but the uniqueness of the proposed method is the new control law. Based on the flatness principle introduced above, the input power of each converter cell p_L is assumed to be the flat output component. Thus, we define a flat output $y=p_L$, a control variable u=d, and a state variable $x=i_L$. From (3), the state variable x can be written as

$$x = \frac{p_L}{v_{\rm FC}} = \varphi(y). \tag{15}$$

From (1) and (7), the control variable u can be calculated from the flat output y and its time derivative \dot{y} , i.e.

$$u = 1 + \left(\dot{y} \cdot \frac{L}{v_{\text{FC}}} + R_L \cdot i_L - v_{\text{FC}}\right) \cdot \frac{1}{v_{\text{Bus}}} = d = \psi(\dot{y}). \tag{16}$$

It is apparent that $x=\varphi(y)$ and $u=\psi(\dot{y})$ correspond to (13) and (14), respectively. Consequently, the mathematical model of the converter can be considered as a flat system.

B. Control Law and Stability

The input-power reference of each module is represented by $y_{\rm REF}$ (= $p_{\rm LREF}$). A linearizing feedback control law achieving an exponential asymptotic tracking of the trajectory is given by the following expression [12], [16]:

$$(\dot{y} - \dot{y}_{REF}) + K_{11}(y - y_{REF}) + K_{12} \int_{0}^{t} (y - y_{REF}) d\tau = 0$$
(17)

where K_{11} and K_{12} are the controller parameters. One may set the following as a desired characteristic polynomial:

$$p(s) = s^2 + 2\zeta\omega_n s + \omega_n^2$$
 $K_{11} = 2\zeta\omega_n$ $K_{12} = \omega_n^2$ (18)

where ζ and ω_n are the desired dominant damping ratio and natural frequency, respectively.

Replacing the term for \dot{y} into (16) gives the equation for the closed-loop static-state feedback duty cycle d (called the inverse dynamic equation), where $e = y - y_{\text{DEC}}$, i.e.

$$u = 1 + \left(\left(\dot{y}_{REF} - K_{11}e - K_{12} \int_{0}^{t} e d\tau \right) - \frac{L}{v_{FC}} + R_L \cdot i_L - v_{FC} \cdot \frac{1}{v_{Bus}} \right)$$

$$= \psi(\dot{y}) = d. \tag{19}$$

Clearly, the control system is stable for K_{11} , $K_{12} > 0$ $(\zeta, \omega_n > 0)$. Thus, the nonlinear-control law of the input power detailed above is portrayed in Fig. 3. The measured

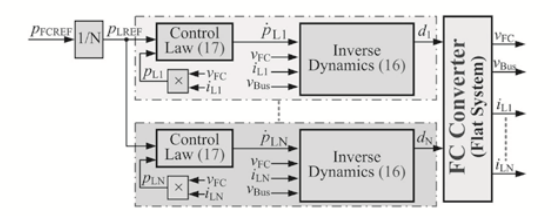


Fig. 3. Power-control loop based on the flatness principle of the multiphase boost converters.

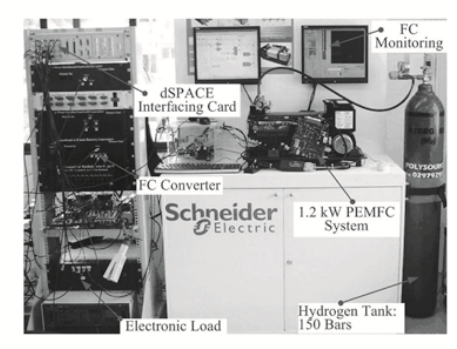


Fig. 4. Photograph of test-bench system.

TABLE I CONVERTER PARAMETERS AND SEMICONDUCTOR DEVICES

Inductors $L_1=L_2=L_3=L_4$	420 μΗ
C_{Bus}	2,700 μ F
$MOSFETs S_1 = S_2 = S_3 = S_4$	IRFP264N: 250 V, 38 A
Diodes $D_1 = D_2 = D_3 = D_4$	RURG3020: 200 V, 30 A

input powers of each module are carried out by means of (3) associated to a first-order filter used to reduce harmonics due to power-electronic switching. Based on the power-electronic constant switching frequency ω_S (PWM) and the cascade control structure, the outer control loop (here, the input-power control) must operate at a cutoff frequency $\omega_P \ll \omega_F$ (a cutoff frequency of the first-order filter) $\ll \omega_S$. Once the flat outputs are stabilized, the whole system is exponentially stable because all the variables of the system are expressed in terms of the flat outputs.

V. EXPERIMENTAL VALIDATION

A. Test-Bench Description

The small-scale test bench was implemented in the laboratory, as presented in Fig. 4. The four-phase boost converter parameters and semiconductor components are detailed in Table I. The FC system used in this effort was a PEMFC system (1.2 kW, 46 A, and based on Ballard Power Systems Inc.), as illustrated in Fig. 4. The power-control loops were implemented in the real-time card dSPACE DS1104 platform (see Fig. 4) using the fourth-order Runge-Kutta integration algorithm and a sampling time of $20~\mu s$, through the mathematical environment of MATLAB–Simulink.

TRF: MRG5380261

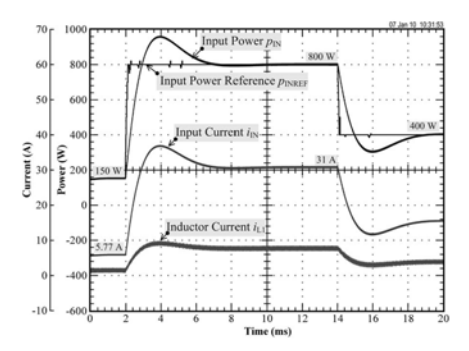


Fig. 5. Dynamic performance at an input-power reference $p_{\rm INREF}$ step from 150 to 800 W at t=2 ms and from 800 to 400 W at t=14 ms.

B. Experimental Results

1) FC Converter Testing With an Ideal Power Supply: Because the FC has slow dynamics by nature [17], an initial testing was performed using an ideal 26-V power supply (which has the same rated voltage as the FC) in place of the FC in order to confirm that the converter can operate correctly and to observe the dynamic performance of the proposed control law.

Fig. 5 presents waveforms that are obtained during the large step of the input-power setpoint. The nonlinear controller gains used were $K_{11}=1414~{\rm rd\cdot s^{-1}}$ and $K_{12}=1\,000\,000~{\rm rd^2\cdot s^{-2}}$ ($\zeta=0.707;~\omega_n=1000~{\rm rd\cdot s^{-1}}$). As a result, the cutoff frequency ω_P of the closed-loop input power was equal to $1000~{\rm rd\cdot s^{-1}}$, which is lower than the cutoff frequency ω_F of the measured power filter of $10\,000~{\rm rd\cdot s^{-1}}$ ($T_F=0.1~{\rm ms}$), so that the system was exponentially stable.

The data show the input-power reference p_{INREF} (instead of p_{FCREF}), the input-power response p_{IN} (instead of p_{FC}), the input current $i_{\rm IN}$ (instead of $i_{\rm FC}$) and the first inductor current i_{L1} . In the initial state, the input-power setpoint is equal to 150 W, the constant input voltage (instead of $v_{\rm FC}$) is equal to 26 V, and the dc bus voltage is equal to 60 V; as a result, the average input current is equal to around 5.77 A (150 W/26 V), and the first inductor current is equal around 1.44 A (150 W/4/26 V). At t=2 ms, the input-power setpoint steps to the constant power of 800 W (positive transition), and at t = 14 ms, the input-power setpoint steps from 800 to 400 W (negative transition). The results reveal that, corresponding to the second-order dynamics [see (18)] of the observation error, the dynamic response is affected by this kind of large input command. The overshoot (no oscillations) in the inputpower response is due to a large proportional gain K_{11} of 1414 rd \cdot s⁻¹ and the vast setpoint step. The value of K_{11} can be reduced to attenuate the overshoot; however, this leads to a slower transition. Therefore, the present mathematical model of the power converter precisely predicts the dynamics of the

2) FC Converter Testing With a PEMFC: Because the FC has slow dynamics by nature, only the constant input-power reference was performed. The oscilloscope waveforms in Fig. 6 portray the steady-state characteristics of the interleaved converters at the FC power reference of 500 W, the electronic load at the dc bus being adjusted in order to obtain a constant dc bus voltage of 60 V (here, the rated value). The data illustrate the

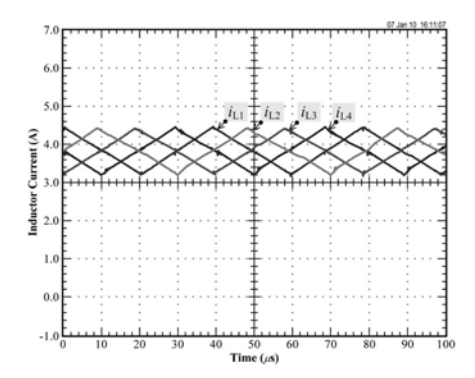


Fig. 6. Inductor-current waveforms of the converter at an FC power reference $p_{\rm FCREF}$ of 500 W ($v_{\rm Bus}=60\,$ V, $v_{\rm FC}=33.00\,$ V, $i_{\rm FC}=15.15$ A, and $i_L=3.79$ A).

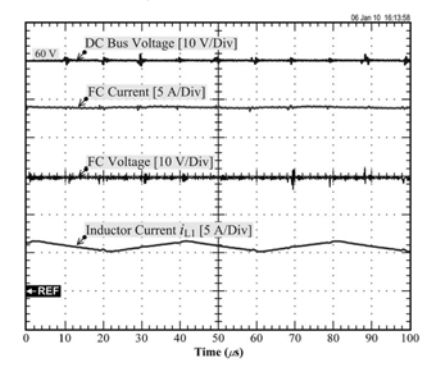


Fig. 7. Steady-state waveforms of the converter at an FC power reference $p_{\rm FCREF}$ of 700 W ($v_{\rm Bus}=60$ V, $v_{\rm FC}=30.00$ V, $i_{\rm FC}=23.80$ A, and $i_L=5.95$ A).

first, the second, the third, and the fourth inductor currents. One can observe that the paralleled interleaving-boost approach uses forced current sharing between the power stages to balance the power that the stages deliver.

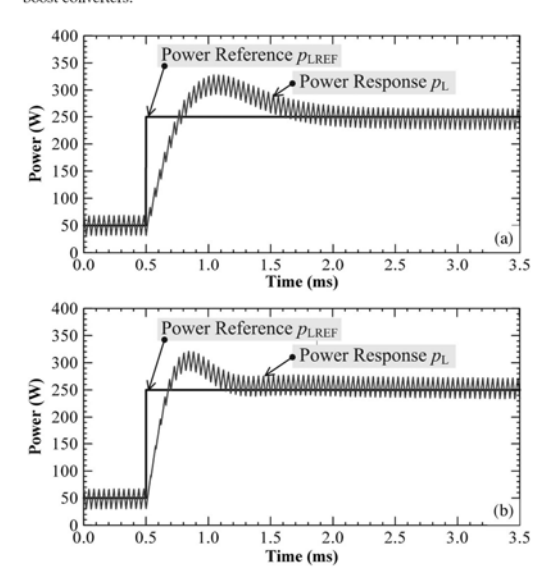
As a final test, oscilloscope waveforms obtained during the FC power demand of 700 W are presented in Fig. 7. The data show the FC current, the dc bus voltage, the FC voltage, and the first inductor current i_{L1} . One can observe that the FC current is the sum of the inductor currents and that the FC ripple current is 1/N of the individual inductor ripple currents. It means that the FC mean current is close to the FC root-mean-square current.

VI. COMPARATIVE STUDY

To compare the performance of the flatness-based control, a traditional linear PI control method is also detailed. However, a current controller is classically implemented [3], [17] in place of the power controller. An inductor-current reference is represented by $i_{\rm LREF}$. A linear feedback PI control law is given by the following expression:

$$d = K_P(i_{\text{LREF}} - i_L) + K_I \int_0^t (i_{\text{LREF}} - i_L) d\tau$$
 (20)

Fig. 8. Power-control loop based on a linear PI principle of the single-phase



Simulation results. Comparison of the flatness-based control law with a linear PI control law. (a) Linear PI and (b) flatness converter resplarge step of the power reference from 50 to 250 W at $t=0.5\,\mathrm{ms}$.

where K_P and K_I are the set of controller parameters. Thus, the linear-control law of the power-control loop is portrayed in Fig. 8. It is similar to the nonlinear-control law (see Fig. 3), where the PI controller also generates a duty-cycle reference d. The main difference between the nonlinear control based on the flatness property and the classical linear control is that the inverse dynamic equation, known as the flatness property [see (16) and Fig. 3], appears in the nonlinear control.

To compare the performance of the flatness-based control and the linear PI control laws, the simulation was implemented. Simulations with MATLAB/Simulink were performed using a switching model of the boost converter. To give a reasonable comparison between the methods, the parameters of the linear PI controller K_P and K_I were tuned to obtain the best possible performance, and this result is compared with the flatness-based control. Then, $K_P = 0.15 \text{ A}^{-1}$, and $K_I = 200 \text{ (A} \cdot \text{s)}^{-1}$.

Fig. 9 shows the simulation results obtained for both controllers during the large step of the power reference. It is similar to the test-bench results illustrated in Fig. 5. The flatness-based control shows a better dynamic response. Although the dynamic response of the linear-control law could be improved relative to that shown in Fig. 9, this enhancement came at the expense of a reduced stability margin. From these results, we conclude that the flatness-based control provides a better performance than the classical PI controller.

VII. CONCLUSION

The main contribution of this brief is to model and control a nonlinear switching-power converter. Distributed power systems often invoke the need to parallel power converters for a variety of reasons, i.e., enhanced reliability, enabling the use of standardized designs with varying loads, distributing heat sources, and improved maintainability. The proposed converter is four-phase parallel step-up converters with the interleaved switching technique. Controlling an interleaved multiphase converter is the same as controlling a single boost converter, but the uniqueness of the proposed method is the new control law. Using the nonlinear-control approach based on the flatness property, we have proposed a simple solution to the optimization and stabilization problems in the nonlinear power-electronic system. This is the novel concept for this kind of application.

REFERENCES

- [1] J. Bernard, S. Delprat, F.-N. Büchi, and T.-M. Guerra, "Fuel-cell hy-brid powertrain: Toward minimization of hydrogen consumption," *IEEE Trans. Veh. Technol.*, vol. 58, no. 7, pp. 3168–3176, Sep. 2009.
 P. Thounthong, B. Davat, S. Raël, and P. Sethakul, "Fuel cell high-
- ower applications," IEEE Ind. Electron. Mag., vol. 3, no. 1, pp. 32-46,
- [3] J. Zou, X. Ma, and C. Du, "Asymmetrical oscillations in digitally con-
- [3] J. Zou, X. Ma, and C. Du, "Asymmetrical oscillations in digitally controlled power-factor-correction boost converters," *IEEE Trans. Circuits Syst. II. Exp. Brief*, vol. 56, no. 3, pp. 230–234, Mar. 2009.
 [4] P. Thounthong, S. Raël, and B. Davat, "Analysis of supercapacitor as second source based on fuel cell power generation," *IEEE Trans. Energy Convers.*, vol. 24, no. 1, pp. 247–255, Mar. 2009.
 [5] S. Ozeri, D. Shmilovitz, S. Singer, and L. M. Salamero, "The mathematical foundation of distributed intelleguage multiple systems," *IEEE Trans. Conference on Control and Conference and Control and Conference and Co*
- ical foundation of distributed interleaved multiple systems," *IEEE Trans. Circuits Syst. I, Reg. Papers*, vol. 54, no. 3, pp. 610–619, Mar. 2007.
 [6] F. Amato, C. Cosentino, A. S. Fiorillo, and A. Merola, "Stabilization of
- [6] F. Albado, C. Coscidino, A. G. Ferrico, and C. F. Albado, C. Coscidino, A. G. Ferrico, and E. F. Linear States Syst. II. Exp. Brief., vol. 56, no. 1, pp. 76–80, Jan. 2009.
 [7] M. Hajian, G. R. Arab Markadeh, J. Soltani, and S. Hoseinnia, "Energy
- M. Hajian, O. K. Arab Markaden, J. Soliani, and S. Hoseinma, Energy optimized sliding-mode control of sensorless induction motor drives," Energy Convers. Manage., vol. 50, no. 9, pp. 2296–2306, Sep. 2009.
 V. Kumar, R. R. Joshi, and R. C. Bansal, "Optimal control of matrix-converter-based WECS for performance enhancement and efficiency optimization," *IEEE Trans. Energy Convers.*, vol. 24, no. 1, pp. 264–273, Mar. 2009. [9] F. U. Syed, M. L. Kuang, M. Smith, S. Okubo, and H. Ying, "Fuzzy gain-
- scheduling proportional-integral control for improving engine power and speed behavior in a hybrid electric vehicle," *IEEE Trans. Veh. Technol.*, vol. 58, no. 1, pp. 69-84, Jan. 2009.
- vol. 58, no. 1, pp. 69–84, Jan. 2009.
 M. Fliess, J. Lévine, Ph. Martin, and P. Rouchon, "A Lie–Bäcklund approach to equivalence and flatness of nonlinear systems," *IEEE Trans. Autom. Control*, vol. 44, no. 5, pp. 922–937, May 1999.
 M. A. Danzer, J. Wilhelm, H. Aschemann, and E. P. Hofer, "Model-based control of a plent for the control of the programment of the pr
- control of cathode pressure and oxygen excess ratio of a PEM fuel cell system," *J. Power Sources*, vol. 176, no. 2, pp. 515–522, Feb. 2008.
 [12] E. Song, A. F. Lynch, and V. Dinavahi, "Experimental validation of non-
- linear control for a voltage source converter," *IEEE Trans. Control Syst. Technol.*, vol. 17, no. 5, pp. 1135–1144, Sep. 2009.
 [13] A. Gensior, H. Sira-Ramirez, J. Rudolph, and H. Guldner, "On some
- nonlinear current controllers for three-phase boost rectifiers," *IEEE Trans. Ind. Electron.*, vol. 56, no. 2, pp. 360–370, Feb. 2009.
 [14] T. Rabbani, S. Munier, D. Dorchies, P. Malaterre, A. Bayen, and
- X. Litrico, "Flatness-based control of open-channel flow in an irrigation canal using SCADA," *IEEE Control Syst. Mag.*, vol. 29, no. 5, pp. 22–30,
- [15] S. K. Agrawal, K. Pathak, J. Franch, R. Lampariello, and G. Hirzinger, "A differentially flat open-chain space robot with arbitrarily oriented joint axes and two momentum wheels at the base," *IEEE Trans. Autom. Control*, vol. 54, no. 9, pp. 2185–2191, Sep. 2009.
- [16] A. Payman, S. Pierfederici, and F. Meibody-Tabar, "Energy control of supercapacitor/fuel cell hybrid power source," *Energy Convers. Manage.*,
- vol. 49, no. 6, pp. 1637–1644, Jun. 2008.
 [17] P. Thounthong, B. Davat, S. Raël, and P. Sethakul, "Fuel starvation:
 Analysis of a PEM fuel cell system," *IEEE Ind. Appl. Mag.*, vol. 15, no. 4, pp. 52-59, Jul./Aug. 2009.

Differential Flatness Based-Control of Wind Generator/Supercapacitor Power Plant

P. Thounthong¹, S. Sikkabut², P. Sethakul³

1,3 Department of Teacher Training in Electrical Engineering

2,3 Thai-French Innovation Institute

King Mongkut's University of Technology North Bangkok

Bangkok, 10800 Thailand, ¹phtt@kmutnb.ac.th

Abstract—This paper presents a system using a supercapacitor storage device to smoothen the output power fluctuation of a variable-speed wind generator. This kind of system is a multiconverter structure and exhibits nonlinear behavior. In this paper, a nonlinear control algorithm based on the flatness properties of the system is proposed. Utilizing the flatness principle, we propose simple solutions to the energy-management and stabilization problems. To authenticate the proposed control laws, a test bench is realized in the laboratory. The control algorithm is digitally implemented by dSPACE controller DS1104. Experimental results with small-scale devices (a wind generator of 500 W and a supercapacitor bank of 100 F, 32 V, and 500 A) corroborate the superb performance during load cycles.

Keywords-converter; current control; flatness based-control; permanent magnet synchronous generator (PMSG); supercapacitor; wind energy

I. INTRODUCTION

Currently, wind power is considered as a potential energy source. Nevertheless, wind power variation due to haphazardly varying wind speed is still a severe problem for distributed generation system. Consequently, it is indispensable to focus the research on the smoothening of wind power variableness. An electric energy storage system is needed to compensate the gap between the output from the wind generator and the load. At the moment, the supercapacitor (or "ultracapacitor") device has received wide consideration as an auxiliary power source.

Fig. 1 depicts the proposed power plant. For high power applications, the wind generator-boost converter combines four-phase parallel boost converters with interleaving (Fig. 2), and the supercapacitor converter (Fig. 3) employs four-phase parallel bidirectional converters with interleaving [1].

This kind of system is a multiconverter connected in cascade. The operation of a multiconverter structure can lead to interactions between the controls of the converters if they are designed separately. Typically, interactions between converters are studied using impedance criteria to investigate the stability of cascaded systems. In this paper, a nonlinear estimation based on the flatness approach of the system is proposed. Flatness provides a convenient framework for meeting a number of performance specifications for the power plant.

This work was supported in part by the Thailand Research Fund (TRF) under Grant MRG5380261, in part by Faculty of Technical Education, and in part by the King Mongkut's University of Technology North Bangkok.

B. Davat

Groupe de Recherche en Electrotechnique et Electronique de Nancy, INPL-Nancy Université, 54510 Nancy, France, Bernard.Davat@ensem.inpl-nancy.fr

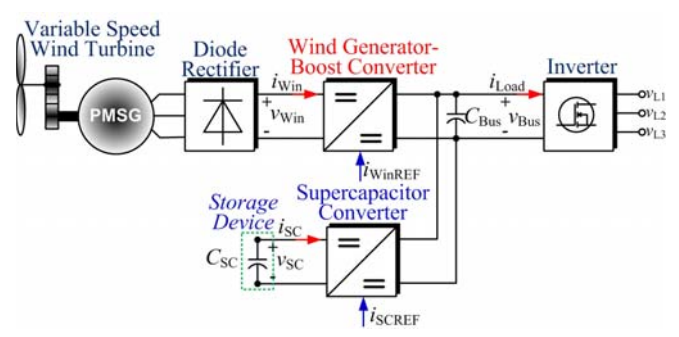


Figure 1. Proposed supercapacitor as a secondary source for the wind generator power plant, where $\nu_{\rm Bus}$ and $i_{\rm Load}$ are the dc-bus voltage and the dc-bus load current, respectively. $\nu_{\rm Win}$ and $i_{\rm Win}$ are the dc output voltage and current from diode rectifier, respectively. $\nu_{\rm SC}$ and $i_{\rm SC}$ are the supercapacitor voltageand current, respectively. $C_{\rm Bus}$ is the total dc bus capacitor.

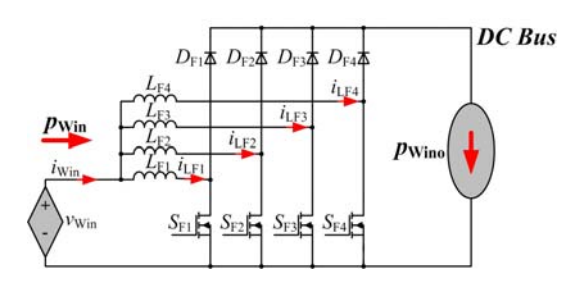


Figure 2. Proposed the wind generator-boost converter, where p_{Win} (= $v_{\text{Win}} \cdot i_{\text{Win}}$) is the wind power and P_{Wino} is the output power from the converter.

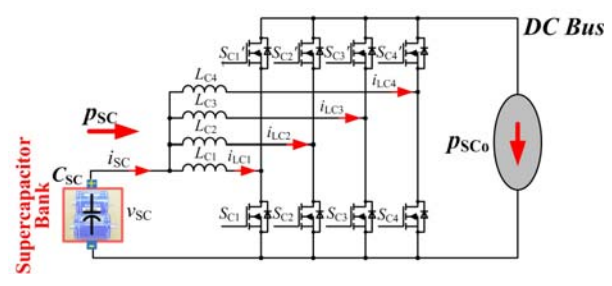


Figure 3. Proposed the bidirectional supercapacitor converter, where $p_{\rm SC}$ (= $v_{\rm SC} \cdot i_{\rm SC}$) is the supercapacitor power and $P_{\rm SCo}$ is the output power from the converter.

II. REDUCED ORDER MODEL OF THE POWER PLANT

For safety and high dynamics, these converters are controlled primarily by inner current regulation loops. These current control loops are supplied by two reference signals: the supercapacitor current reference i_{SCREF} and the dc wind generator current reference i_{WinREF} generated by the energy management algorithm presented hereafter.

One supposes that the input currents follow their set-point values perfectly. Thus

$$i_{\text{Win}} = i_{\text{WinREF}} = \frac{p_{\text{Win}}}{v_{\text{Win}}}, \quad i_{\text{SC}} = i_{\text{SCREF}} = \frac{p_{\text{SC}}}{v_{\text{SC}}}$$
 (1)

The dc-bus capacitive energy $E_{\rm Bus}$ and the supercapacitive energy $E_{\rm SC}$ can be written as

$$E_{\text{Bus}} = \frac{1}{2} C_{\text{Bus}} v_{\text{Bus}}^2, \quad E_{\text{SC}} = \frac{1}{2} C_{\text{SC}} v_{\text{SC}}^2$$
 (2)

The total electrostatic energy $E_{\rm T}$ stored in the dc-bus capacitor and in the supercapacitor can also be written as

$$E_{\rm T} = \frac{1}{2} C_{\rm Bus} v_{\rm Bus}^2 + \frac{1}{2} C_{\rm SC} v_{\rm SC}^2$$
 (3)

The dc-bus capacitive energy $E_{\rm Bus}$ is given versus $p_{\rm Wino}$, $p_{\rm SCo}$, and $p_{\rm Load}$ by the following differential equation, refer to Figs. 1, 2 and 3:

$$\dot{E}_{\rm Bus} = p_{\rm Wino} + p_{\rm SCo} - p_{\rm Load} \tag{4}$$

where,

$$p_{\text{Wino}} = p_{\text{Win}} - r_{\text{Win}} \left(\frac{p_{\text{Win}}}{v_{\text{Win}}} \right)^2, \ p_{\text{SCo}} = p_{\text{SC}} - r_{\text{SC}} \left(\frac{p_{\text{SC}}}{v_{\text{SC}}} \right)^2$$
(5)

$$p_{\rm Load} = \sqrt{\frac{2E_{\rm Bus}}{C_{\rm Bus}}} \cdot i_{\rm Load}, \ p_{\rm SC} = v_{\rm SC} \cdot i_{\rm SC} = \sqrt{\frac{2E_{\rm SC}}{C_{\rm SC}}} \cdot i_{\rm SC} \ \ (6)$$

Note that there are only static losses in these converters (called *reduced order model*), and $r_{\rm win}$ and $r_{\rm sc}$ represent the static losses in the wind generator-boost converter and supercapacitor converter, respectively.

III. CONTROL OF WIND GENERATOR/SUPERCAPACITOR POWER PLANT

In the proposed system depicted in Fig. 1, there are two voltage variables (or two energy variables) to be regulated.

- The dc bus energy $E_{\rm Bus}$ is the most essential variable.
- The supercapacitor storage energy E_{SC} is the next most significant.

Therefore, we propose utilizing supercapacitors, which are the faster energy source in the proposed system, to supply the energy for the dc bus. In fact, we plan to functionalize the wind generator by supplying energy only for charging the supercapacitor $C_{\rm SC}$. However, during charging, the energy for the wind generator flows through the dc bus to the supercapacitor bank. For this reason, the wind generator is mathematically operated to supply energy for both the dc bus capacitor $C_{\rm Bus}$ and the supercapacitor $C_{\rm SC}$ to keep them charged.

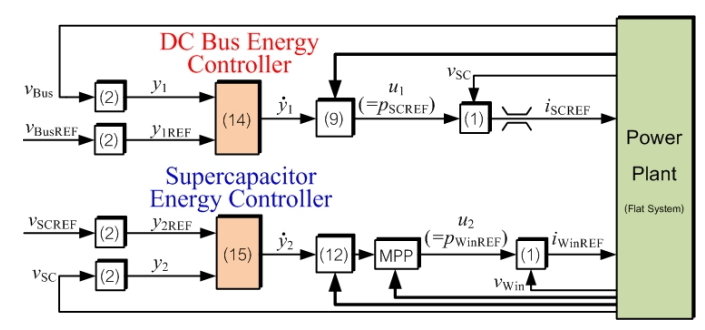


Figure 4. Control of a wind generator/supercapacitor power plant

A. Differential Flatness Property of the Power Plant

Let us first reveal a physical property, used to establish the system flatness [2], that will be the main concept for our reference generations. The flat outputs y, the control input variables u and the state variables x are defined as

$$\mathbf{y} = \begin{bmatrix} y_1 \\ y_2 \end{bmatrix} = \begin{bmatrix} E_{\text{Bus}} \\ E_{\text{T}} \end{bmatrix}, \mathbf{u} = \begin{bmatrix} u_1 \\ u_2 \end{bmatrix} = \begin{bmatrix} p_{\text{SCREF}} \\ p_{\text{WinREF}} \end{bmatrix}, \mathbf{x} = \begin{bmatrix} x_1 \\ x_2 \end{bmatrix} = \begin{bmatrix} v_{\text{Bus}} \\ v_{\text{SC}} \end{bmatrix}$$
(7)

From (2) and (4), the dc bus voltage $v_{\rm Bus}$ and the supercapacitor power can be expressed as

$$x_1 = \sqrt{\frac{2y_1}{C_{\text{Bus}}}} = \varphi_1(y_1)$$
 (8)

$$u_1 = 2p_{\text{SCLim}} \cdot \left[1 - \sqrt{1 - \left(\frac{\dot{y}_1 + i_{\text{Load}} \cdot \varphi_1(y_1) - p_{\text{Wino}}}{p_{\text{SCLim}}} \right)} \right]$$
(9)

$$= \psi_1(y_1, \dot{y}_1) = p_{\text{SCREF}}$$

$$p_{\text{SCLim}} = \frac{v_{\text{SC}}^2}{4r_{\text{SC}}},\tag{10}$$

where p_{SCLim} is the limited maximum power from the supercapacitor converter.

From (3) and (4), the supercapacitor voltage v_{SC} and the wind power p_{Win} can be expressed as an algebraic function

$$x_2 = \sqrt{\frac{2(y_2 - y_1)}{C_{SC}}} = \varphi_2(y_1, y_2)$$
 (11)

$$u_2 = 2p_{\text{WinLim}} \cdot \left[1 - \sqrt{1 - \left(\frac{\dot{y}_2 + i_{\text{Load}} \cdot \varphi_1(y_1)}{p_{\text{WinLim}}} \right)} \right]$$
 (12)

$$= \psi_2(y_1, \dot{y}_2) = p_{\text{WinREF}}$$

$$p_{\text{WinLim}} = \frac{v_{\text{Win}}^2}{4r_{\text{Win}}},\tag{13}$$

where P_{WinLim} is the limited maximum power from the wind generator-boost converter.

It is clear that $x_1 = \varphi_1(y_1)$, $x_2 = \varphi_2(y_1, y_2)$, $u_1 = \psi_1(y_1, \dot{y}_1)$, and $u_2 = \psi_2(y_1, \dot{y}_2)$. Consequently, the proposed power plant can be considered a flat system [2].

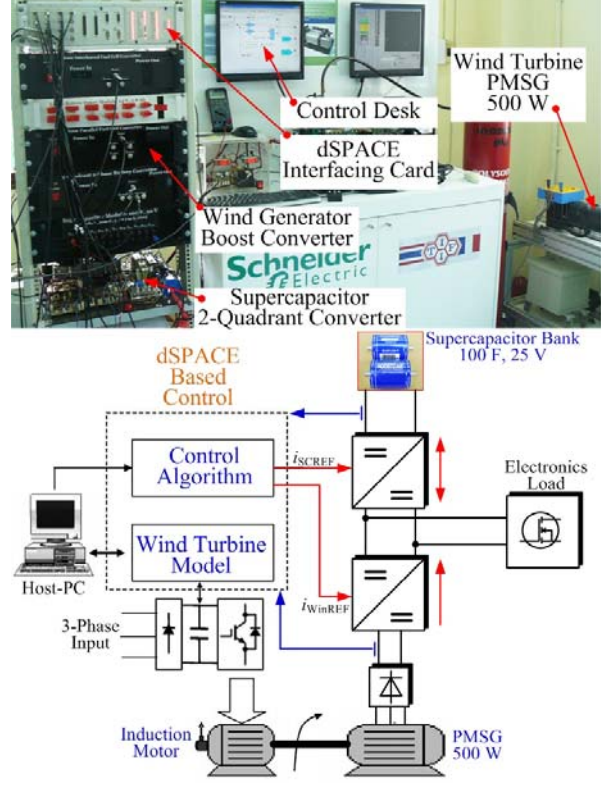


Figure 5. Experimental setup

B. Control Law and Stability

We aim to design a feedback law such that the tracking error $(y_1-y_{1REF}, y_2-y_{2REF})$ asymptotically vanishes. Thus, the relative degree of the first input v_1 and the second input v_2 are two and one, respectively. The proposed control laws [2] are

$$v_{1} = \dot{y}_{1} = \dot{y}_{1REF} + K_{11}(y_{1REF} - y_{1}) + K_{12} \int_{0}^{t} (y_{1REF} - y_{1}) d\tau$$
 (14)
$$v_{2} = \dot{y}_{2} = \dot{y}_{2REF} + K_{21}(y_{2REF} - y_{2}).$$
 (15)

Substituting the expression for \dot{y}_1 into (9) gives the equation for the closed-loop static state feedback supercapacitor power. Substituting the expression for \dot{y}_2 into (12) gives the equation for the closed-loop static state feedback wind power. It is clear that the control system is asymptotically stable for K_{11} , $K_{12} > 0$ and $K_{21} > 0$. Once the flat outputs are stabilized, the whole system is exponentially stable because all of the variables of the system are expressed in terms of the flat outputs.

Fig. 4 depicts the proposed control algorithm of the power plant, as detailed above. The dc-bus energy control law generates a supercapacitor power reference p_{SCREF} (= u_1 , refer to (9)). The total energy control law (or the supercapacitor energy control) generates a wind power demand p_{WinREF} (= u_2 , refer to (12)). This signal must be saturated at the maximum power point MPP by the maximum power point tracking MPPT. Note that it is beyond the scope of this paper to present MPPT of the wind power.

IV. EXPERIMENTAL VALIDATION

The small-scale test bench of the power plant was implemented in our laboratory, as presented in Fig. 5. The prototype 0.5-kW wind generator-boost converter and the 2-kW supercapacitor converter (refer to Figs. 1, 2 and 3) were implemented in the laboratory. The permanent magnet synchronous generator is 500 W and supercapacitor module is 100 F, 32 V. The power plant parameters are $C_{\rm Bus} = 12~200~\mu{\rm F}$, $r_{\rm Win} = 0.12$, and $r_{\rm SC} = 0.10~\Omega$.

For the low-scale test bench, the dc bus voltage reference $v_{\rm BusREF}$ was set to 60 V and the supercapacitor voltage reference $v_{\rm SCREF}$ was set to 25 V (the nominal value of the supercapacitor bank). The controller gains used were $K_{11} = 141 \, {\rm rad \cdot s^{-1}}$, $K_{12} = 10 \, 000 \, {\rm rad}^2 \cdot {\rm s^{-2}}$, and $K_{21} = 0.1 \, {\rm W \cdot J^{-1}}$.

The variable-speed wind turbine is emulated using a speed-regulated cage induction motor. To implement the emulation, a wind speed profile is sent from the host PC. The PMSG rotates at the same speed as that of a generator driven by a real wind turbine.

Waveforms obtained during the load cycle are presented in Fig. 6. The data show the dc bus voltage, the wind speed, the load power, the supercapacitor power, the wind power, the supercapacitor current, and the supercapacitor voltage (or the supercapacitor state-of-charge SOC). In the initial state, the wind speed is 12 m·s⁻¹, the load power is zero, and the storage device is fully charge, i.e., $v_{SC} = 25$ V; as a result, both the wind and supercapacitor powers are zero. At t = 20 s, the load power steps to the final constant power of around 560W (positive load power transition). The following observations are made:

- The supercapacitor supplies most of the 560 W power that is required during the transient step load.
- Synchronously, the wind power increases to a maximum power point (MPP) of around 400 W (at the wind speed is 12 m·s⁻¹), which is limited by the maximum power point tracker (MPPT).
- The input from the supercapacitor, which supplies most of the transient power that is required during the stepped load, slowly decreases and the unit remains in a discharge state after the load step because the steadystate load power is greater than the power supplied by the wind generator.

At t = 48 s to 60 s, the wind speed reduces linearly from 12 m·s⁻¹ to 7.5 m·s⁻¹; as a result, the maximum wind power is reduced from 400 W to 280 W, and then the supercapacitor power supplies more power for the constant load power demanded. At t = 72 s, the load power steps from 560 W to 180 W (negative load power transition). The maximum wind power is over than the load power; as a result, the supercapacitor changes from discharging to charging. The wind generator supplies its maximum power to drive the load and to charge the supercapacitor.

To demonstrate dynamic regulation of the dc-bus energy (voltage, the main important variable), the oscilloscope waveforms in Fig. 7 show the dc bus voltage dynamics to the large load power demanded (disturbance) from 0 to 700 W,

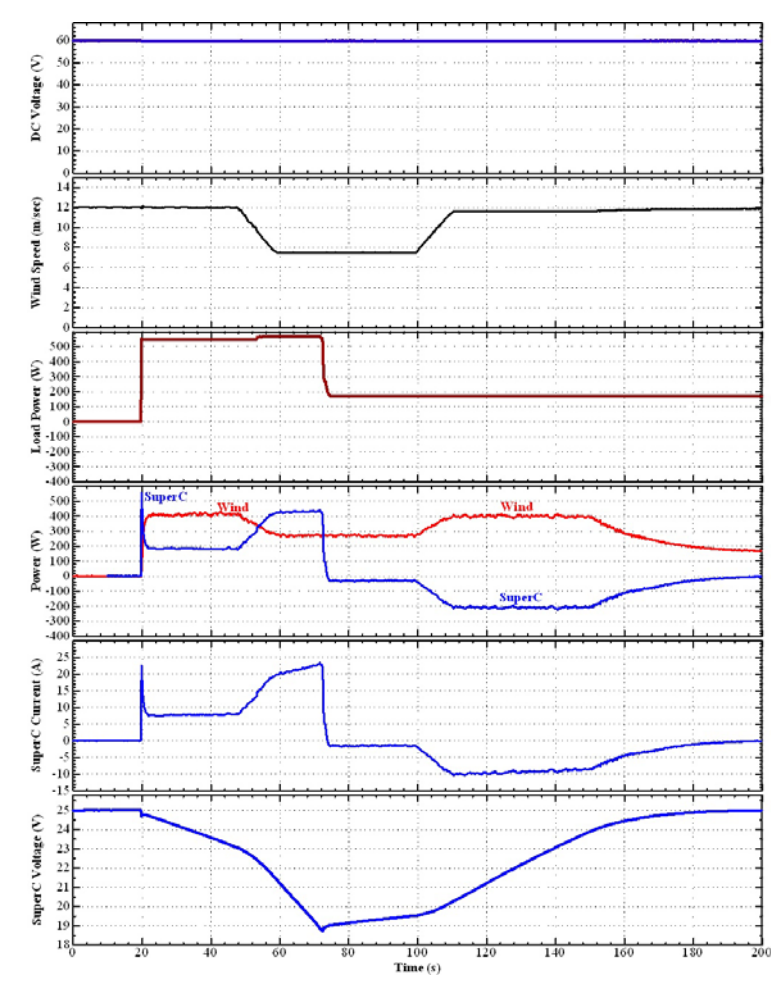


Figure 6. Power plant response during load cycle

whereas the dc bus was loaded with an electronic load. The oscilloscope screens show the dc bus voltage, the supercapacitor voltage, the load power, and the supercapacitor power. Once again, the supercapacitor supplies most of the power that is required during the step load. The experimental results reveal only small perturbations on the dc-bus voltage waveform, which is of key significance by using the flatness-based control law for the dc-bus energy regulation in the proposed system.

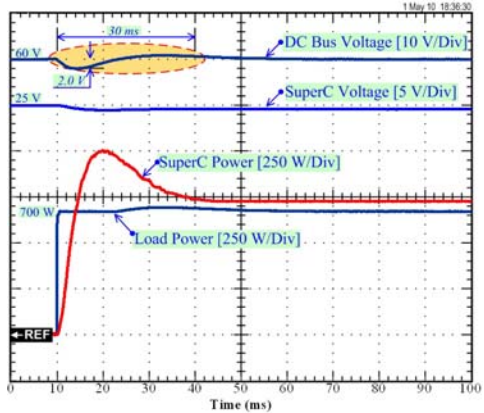


Figure 7. Dynamic characteristic of the power source during a step load from 0 to 700 W.

V. CONCLUSION

In this paper, a supercapacitor storage device has been proposed to smoothen the dc bus voltage fluctuation of a wind generator composed of variable-speed permanent-magnet generators. The control approach, based on the differential flatness control, presents the stability, and efficiency of the distributed generation system.

Experimental results in the laboratory carried out using a small-scale test bench, which employs a wind generator (500 W), and a storage device of supercapacitor bank (100 F, 30 V) authenticate the brilliant performances during load cycles.

REFERENCES

- P. Thounthong, B. Davat, S. Raël, and P. Sethakul, "Fuel cell highpower applications," *IEEE Ind. Electron. Mag.*, vol. 3, no. 1, pp. 32-46, March 2009.
- [2] E. Song, A. F. Lynch, and V. Dinavahi. "Experimental validation of nonlinear control for a voltage source converter," *IEEE Trans. Control Syst. Technol.*, vol. 17, no. 5, pp. 1135–1144, Sept. 2009.
- [3] A. Gensior, H. Sira-Ramirez, J. Rudolph, H. Guldner, "On some nonlinear current controllers for three-phase boost rectifiers," *IEEE Trans. Ind. Electron.*, vol. 56, no. 2, pp. 360–370, Feb. 2009.

Model Based-Control of Three-Level Boost Converter for Fuel Cell Applications

P. Thounthong¹, S. Sikkabut², P. Sethakul³

1,3</sup>Department of Teacher Training in Electrical Engineering

2,3 Thai-French Innovation Institute

King Mongkut's University of Technology North Bangkok

Bangkok, 10800 Thailand, ¹phtt@kmutnb.ac.th

Abstract—This paper presents a high-gain boost converter for an fuel cell (FC) applications. A model-based control structure based-on flatness principle for a distributed dc generation is studied. As the derived dynamic model of the converter model is nonlinear, advanced control techniques using differential flatness are applied. Utilizing the flatness property, we propose simple solutions to the system performance and stabilization problems. Design controller parameters are straightforward and autonomous of the operating point. To validate the proposed method, a prototype FC power converter (1.2-kW three-level boost converter) is realized in the laboratory. The proposed control law is implemented by digital estimation in a dSPACE 1104 controller card. Experimental results with a polymer electrolyte membrane FC of 1200 W and 46 A in the laboratory substantiate the good control scheme.

Keywords-converters; flatness-based control; fuel cells (FCs); nonlinear; power control

I. INTRODUCTION

FCs produce low dc voltage, and they are always connected to electric power networks through a step-up (boost) converter. Theoretically, conventional boost converters are able to achieve high step-up voltage gain in heavy duty load conditions. In practice, however, the voltage gain of the boost converter is limited owing to the losses associated with the inductor, filter capacitor, main power switch and rectifier diode [1].

In many applications, the use of an isolation transformer can provide increased output/input voltage conversion ratio, as required and full-bridge topologies can be used. However, there are applications where transformer-less energy converter systems could potentially offer significant advantages, including simplicity, cost, and converter size reduction, particularly in high power applications [2].

In this paper, a three-level step-up converter (transformer-less) is proposed to solve the problems encountered in the modified boost converters mentioned above. The power electronic converter is a nonlinear behavior. Classically, to control the voltage, the current, or the power in the converter, a linearized technique is often used to study the stability and to select the controller parameters of the nonlinear converter. In this paper, a nonlinear-control algorithm based on the flatness property of the system is proposed. Flatness provides a con-

This work was supported in part by the Thailand Research Fund (TRF) under Grant MRG5380261, in part by Faculty of Technical Education under Grant FTE-2554-14, and in part by the King Mongkut's University of Technology North Bangkok.

B. Davat

Groupe de Recherche en Electrotechnique et Electronique de Nancy, INPL-Nancy Université, 54510 Nancy, France, Bernard.Davat@ensem.inpl-nancy.fr

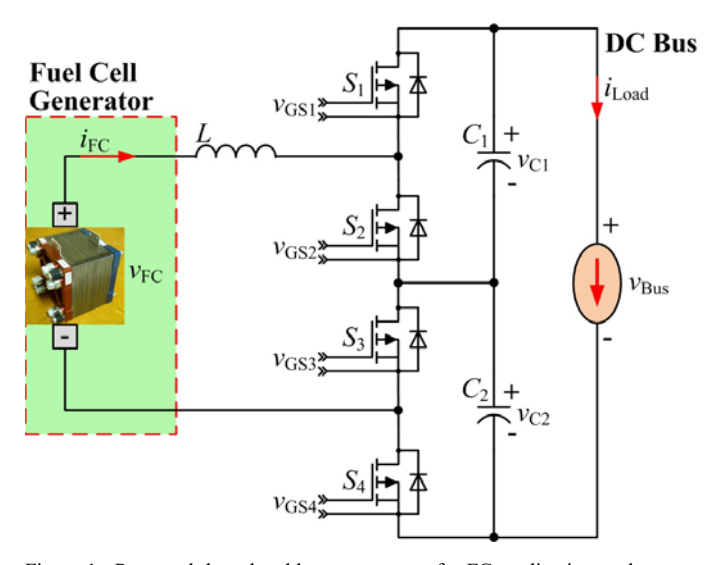


Figure 1. Proposed three-level boost converter for FC applications, where $\nu_{\rm FC}$ and $i_{\rm FC}$ are the FC voltage and current, respectively. $i_{\rm Load}$ is the load current. $\nu_{\rm Bus}$ the dc bus voltage.

venient framework for meeting a number of performance specifications on the power converter. This paper is organized as follows. Section II shows the proposed power converter circuit and the average model. Section III discusses the proof of differential flatness of the proposed FC converter models and the control law and stability. Experimental results will authenticate the proposed control system in Section IV. Finally, this paper ends with concluding remarks in Section V.

II. THREE LEVEL BOOST CONVERTER

A. Power Circuit

FC operates giving direct current, and at a low voltage; thereby, the boost converter is always selected to adapt the low dc voltage delivered by the FC to the higher dc-bus voltage level [2]. A classical boost converter will be limited when the power increases or for higher voltage step-up ratios. To increase the higher voltage conversion ratio, Grbović *et al.* [3] has proposed the three-level boost converters (transformer-less power converter) for a low voltage power source, as shown in Fig. 1.

The FC current ripple reduction is a major issue for FC converter design [1]. The proposed configuration was chosen instead of the conventional boost converter of the smaller size of the inductor needed to achieve comparably low ripple [2]. In addition, it reduces the required semiconductor device voltage rating by a factor of two.

By cascading the output voltage $v_{\rm C1}$ and the output voltage $v_{\rm C2}$, high output voltage $v_{\rm Bus}$ is easily obtained. In addition, there is low voltage stress on the power switch and diode as well as on the output capacitors compared to that for conventional boost converters. Therefore, the converter's overall performance, including cost and efficiency, can significantly be better compared to two-level converters, especially when the switching frequency $f_{\rm S}$ (= $1/T_{\rm S}$) is above 20 kHz or metal—oxide—semiconductor field-effect transistors MOSFETs are used.

The switching functions (Fig. 2) are generated by the pulsewidth modulators PWM₁ and PWM₂ and $T_{\rm S}$ is the switching period. The modulation signals d_1 and d_2 (> 0.5) are duty cycles generated by a control circuit (current control or power control loop presented hereafter). The carrier signals are triangular signals $v_{\rm Car1}$ and $v_{\rm Car2}$ shifted for π (called interleaving technique).

B. Average Model

The output capacitors C_1 and C_2 are assumed to be large enough so that the output voltages v_{C1} and v_{C2} across them are considered as constant during the entire switching cycle, and become $v_{\text{Bus}} = v_{\text{C1}} + v_{\text{C2}}$. Adopted from the average model of a conventional boost converter, the circuit can be described by the following set of equations:

$$L\frac{d\overline{i}_{FC}}{dt} = \overline{v}_{FC} - r_L \cdot \overline{i}_{FC} - (1 - d_1) \cdot \overline{v}_{C1} - (1 - d_2) \cdot \overline{v}_{C2}$$
 (1)

$$C_1 \frac{d\overline{v}_{C1}}{dt} = (1 - d_1) \cdot \overline{i}_{FC} - i_{Load}$$
 (2)

$$C_2 \frac{d\overline{v}_{C2}}{dt} = (1 - d_2) \cdot \overline{i}_{FC} - i_{Load}$$
 (3)

where $r_{\rm L}$ is the series resistance of inductor L. Note that $r_{\rm L}$ also represents the static losses in the converter. One assumes that the filter capacitors are taken to be identical, i.e., $C_1 = C_2 = C$, and $d_1 = d_2 = d$ and $v_{\rm C1} = v_{\rm C2} = v_{\rm Bus}/2$. From (1), the differential equation can be written as

$$L\frac{d\bar{i}_{FC}}{dt} = \bar{v}_{FC} - r_{L} \cdot \bar{i}_{FC} - (1 - d) \cdot \bar{v}_{Bus}$$
 (4)

The input power p_{FC} is given versus v_{FC} and i_{FC} by the following differential equation:

$$\overline{p}_{FC} = \overline{v}_{FC} \cdot i_{FC} \tag{5}$$

$$\left. \frac{d\bar{p}_{FC}}{dt} = v_{FC} \frac{d\bar{i}_{FC}}{dt} \right|_{\bar{v}_{FC} = \text{Constant}} . \tag{6}$$

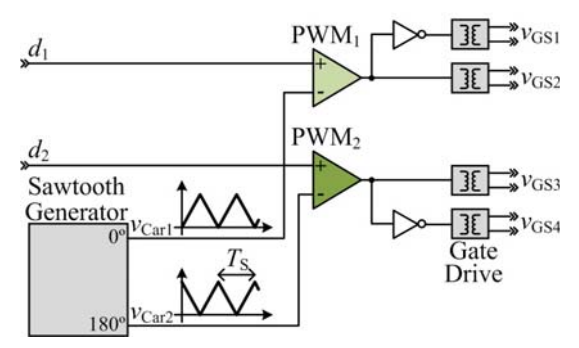


Figure 2. Switching functions of the proposed converter with phase shifted for π

III. POWER CONTROL LOOP

A. Flatness of the Proposed Converter

The FC power p_{FC} is assumed to be the flat output component. Thus, we define a flat output $y = p_{FC}$, a control input variable u = d, and a state variable $x = i_{FC}$. The state variable x can be written as

$$x = \frac{p_{FC}}{v_{FC}} = \varphi(y). \tag{7}$$

From (4) and (6), the control variable u can be calculated from the flat output y and its time derivative \dot{y} , i.e.

$$u = 1 + \left(\dot{y} \cdot \frac{L}{v_{FC}} + r_{L} \cdot i_{FC} - v_{FC}\right) \cdot \frac{1}{v_{Bus}} = d = \psi(\dot{y})$$
 (8)

It is clear that $x = \varphi(y)$ and $u = \psi(\dot{y})$. Consequently, the mathematical model of the converter can be considered as a flat system [4], [5].

B. Control Law and Stability

The input-power reference of converter is represented by y_{REF} (= p_{FCREF}). A linearizing feedback control law achieving an exponential asymptotic tracking of the trajectory is given by the following expression [4], [5]:

$$(\dot{y} - \dot{y}_{REF}) + K_{11}(y - y_{REF}) + K_{12} \int (y - y_{REF}) d\tau = 0$$
 (9)

where K_{11} and K_{12} are the controller parameters. Then,

$$\dot{y} = \dot{y}_{REF} + K_{11}(y_{REF} - y) + K_{12} \int (y_{REF} - y) d\tau$$
 (10)

Replacing the term for \dot{y} into (8) gives the equation for the closed-loop static-state feedback duty cycle d (called the *inverse dynamic equation*). Evidently, the control system is stable for K_{11} , $K_{12} > 0$. Once the flat outputs are stabilized, the whole system is exponentially stable because all the variables of the system are expressed in terms of the flat outputs [4].

C. Balance Voltage in the Output Capacitors

Voltage balancing controller functions to eliminate the difference between voltages v_{C1} and v_{C2} . The duty cycles d_1 and d_2 are determined as

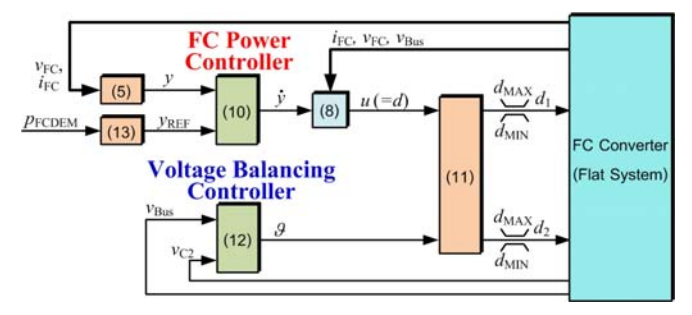


Figure 3. Proposed FC power control scheme for the three-level converter.

$$d_1 = d - \vartheta$$

$$d_2 = d + \vartheta$$
(11)

where d is the main duty cycle generated by the power controller (refer to (8)) and ϑ represents a correction term, in order to balance the voltages.

A proportional controller is sufficient, as far as the gain is high enough to introduce only a little static error. Therefore, the voltage balancing control can be expressed by the following function:

$$\vartheta = K_{\rm v}(\frac{v_{\rm Bus}}{2} - v_{\rm C2}) \tag{12}$$

where K_V is the controller parameter.

D. Conclusion of the Control Algorithm

The FC power reference $p_{\rm FCREF}$ must be limited in dynamics; these limitations ensure safe operation of the FC with respect to the constraints that are associated with the FC (i.e., the prevention of an FC stack from undergoing fuel starvation [2]). Thus, to limit the transient FC power, a low-pass filter (second order) is employed such that the power demand $p_{\rm FCDEM}$ from external loop is always limited (planning desired trajectory) by,

$$p_{\text{FCREF}}(t) = p_{\text{FCDEM}}(t) \cdot (1 - e^{-\frac{t}{\tau_1}} - \frac{t}{\tau_1} e^{-\frac{t}{\tau_1}})$$
 (13)

where τ_1 is the control parameter.

Thus, the model based-control law based on the differential flatness approach of the FC power detailed above is portrayed in Fig. 3.

IV. EXPERIMENTAL VALIDATION

The small-scale test bench was implemented in the laboratory, as presented in Fig. 4. The three-level boost converter parameters and semiconductor components are detailed in Table I. The FC system used in this effort was a PEMFC system (1.2 kW, 46 A, and based on Ballard Power Systems Inc.), as illustrated in Fig. 4. The FC power control loop, the voltage balancing control, and the PWM generation algorithm were implemented in the real-time card dSPACE DS1104 platform (see Fig. 4) using the fourth-order *Runge–Kutta* integration algorithm and a sampling time of 20 μ s. The switching frequency $f_{\rm S}$ was set at 10 kHz.

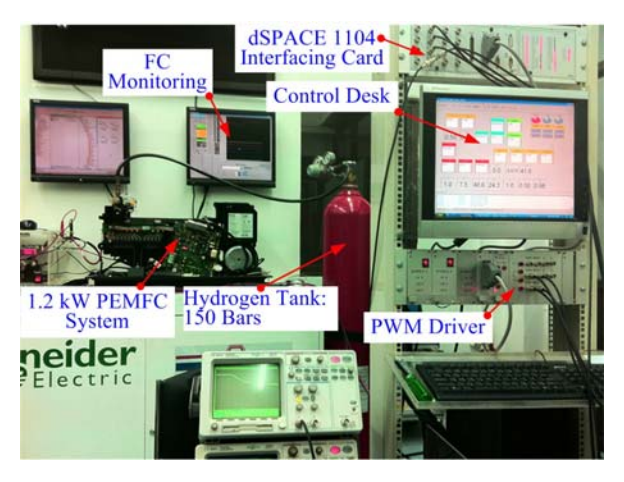


Figure 4. Test bench system.

TABLE I CONVERTER PARAMETERS AND SEMICONDUCTOR DEVICES

Inductor L	223	μΗ
Series resistance $r_{\rm L}$	0.14	Ω
Capacitors C_1 , C_2	1,000	μ F
$MOSFETs S_1 = S_2 = S_3 = S_4$	IRFP264N: 250 V, 38 A	

The nonlinear controller gains used were $K_{11} = 141.4 \text{ rd} \cdot \text{s}^{-1}$ and $K_{12} = 10~000 \text{ rd}^2 \cdot \text{s}^{-2}$. The voltage balancing controller gain was $K_{V} = 0.6$. The parameter τ_{1} for the FC power dynamic (planning desired trajectory) was 5 s. This value has experimentally been determined as the highest power slope of our FC system, where no fuel starvation occurs.

To illustrate the switching characteristics of the proposed converter, the oscilloscope waveforms in Fig. 5 portray the steady-state wave forms at the FC power regulation at the power reference of 500 W. It shows the FC voltage v_{FC} (CH1), the FC current i_{FC} (CH2), the gate drive signal for S_2 v_{GS2} (CH3), and the gate drive signal for S_3 v_{GS3} (CH4). The power switching devices, S_2 and S_3 , (individual interleaved power stages) operate at the same frequency as the classical boost converter design, 10 kHz, but the effective input FC current-ripple frequency is 20 kHz; as a result, the FC ripple current is reduced.

Waveforms obtained during the increasing of the FC power reference trajectory $p_{\rm FCREF}$ are presented in Fig. 6. The data show the FC power reference trajectory $p_{\rm FCREF}$ (CH1), the measured FC power $p_{\rm FC}$ (CH2), the FC voltage $v_{\rm FC}$ (CH3), and the FC current $i_{\rm FC}$ (CH4). In the initial state, the FC power reference is equal to 200 W, the measured FC power is equal to 200 W, the FC voltage is equal to 36.4 V, and the FC current is equal to 5.5 A. At t=5 s, the FC power reference trajectory slowly increases to the final constant power of 500W. The measured FC power follows its reference perfectly, and there is no fuel starvation phenomenon in the FC system, because the FC power reference trajectory is limited the dynamics, refer to (13).

Finally, waveforms obtained during the decreasing of the FC power reference trajectory p_{FCREF} are presented in Fig. 7.